Developmental Biology 340 (2010) 381–396

Contents lists available at ScienceDirect

Developmental Biology

journal homepage: www.elsevier.com/developmentalbiology

The Pax3 and Pax7 paralogs cooperate in neural and neural crest patterning using distinct molecular mechanisms, in *Xenopus laevis* embryos

Frédérique Maczkowiak [a,b,c], Stéphanie Matéos [a,b], Estee Wang [d], Daniel Roche [a,b,c], Richard Harland [d], Anne H. Monsoro-Burq [a,b,c,*]

[a] Institut Curie, Centre de Recherche, Centre Universitaire, F-91405 Orsay, France
[b] CNRS UMR 3347, INSERM U1021, Orsay, France
[c] Université Paris Sud-11, Orsay, France
[d] UC Berkeley, MCB Department, USA

ARTICLE INFO

Article history:
Received for publication 16 September 2009
Revised 6 January 2010
Accepted 20 January 2010
Available online 29 January 2010

Keywords:
Pax3
Pax7
Brain
Neural crest
Mesoderm
FGF
WNT
Otx2
Krox20
Snail2
Patterning

ABSTRACT

Pax3 and Pax7 paralogous genes have functionally diverged in vertebrate evolution, creating opportunity for a new distribution of roles between the two genes and the evolution of novel functions. Here we focus on the regulation and function of Pax7 in the brain and neural crest of amphibian embryos, which display a different *pax7* expression pattern, compared to the other vertebrates already described. *Pax7* expression is restricted to the midbrain, hindbrain and anterior spinal cord, and Pax7 activity is important for maintaining the fates of these regions, by restricting *otx2* expression anteriorly. In contrast, *pax3* displays broader expression along the entire neuraxis and Pax3 function is important for posterior brain patterning without acting on *otx2* expression. Moreover, while both genes are essential for neural crest patterning, we show that they do so using two distinct mechanisms: Pax3 acts within the ectoderm which will be induced into neural crest, while Pax7 is essential for the inducing activity of the paraxial mesoderm towards the prospective neural crest.

Introduction

Pax3 and Pax7 are members of the Pax family of transcriptional regulators. They contain two DNA binding domains, a paired domain and a paired-type homeodomain (Chalepakis et al., 1994a,b; Gruss and Walther, 1992; Jostes et al., 1990). Human syndromes with Pax3 mutations (Waardenburg syndrome types I and III) and mouse mutants (Splotch/Pax3 mutant and Pax7 mutant) have highlighted their prominent roles in early embryogenesis and during adulthood (Chalepakis et al., 1994a; Epstein et al., 1991; Read and Newton, 1997; Tassabehji et al., 1992). In adults, they are essential in muscle homeostasis and repair (Buckingham, 2006; Kuang and Rudnicki, 2008; Le Grand and Rudnicki, 2007). In embryos, they are major regulators of central nervous system, neural crest and paraxial mesoderm patterning and differentiation. During vertebrate evolution, Pax3 and Pax7 duplicated from an ancestral gene (Holland et al., 1999; McCauley and Bronner-Fraser, 2002; Osorio et al., 2005). Further duplications have occurred in zebrafish, which has four genes: Pax3/Pax3b and Pax7/Pax7b (Thompson et al., 2008). While such gene duplications may retain functional overlap between Pax3 and Pax7, they also open the possibility for distribution of the various functions assumed by the ancestral gene and the evolution of novel functions for each paralog. Indeed, the comparison of Pax3 and Pax7 gene expression shows differences between vertebrates (see below). The analysis of the functional implications of such differences reveals distinct functions between Pax3 and Pax7 in various cell types, such as muscle or neuron progenitors (Relaix et al., 2004; Thompson et al., 2008).

Here we focus on the early mechanisms of neural and neural crest development. During mouse, chick and fish neurulation and organogenesis, *Pax3* and *Pax7* are both expressed in overlapping patterns in the central nervous system, including expression in the mesencephalon, the hindbrain and the spinal cord, with some subtle regional differences between the two genes (Borycki et al., 1999; Goulding et al., 1994a; Mansouri et al., 1996; Minchin and Hughes, 2008; Thompson et al., 2008). In their various locations along the anterior–posterior axis, *Pax3* and *Pax7* domains of expression are restricted to the dorsal part of the central nervous system. Ventral midline-derived signals, such as sonic hedgehog and noggin, restrict their expression

* Corresponding author. CNRS UMR 3347, INSERM U1021, Institut Curie, Centre Universitaire, Batiment 110, F-91405 Orsay cedex, France.
E-mail address: anne-helene.monsoro-burq@curie.u-psud.fr (A.H. Monsoro-Burq).

0012-1606/$ – see front matter © 2010 Elsevier Inc. All rights reserved.
doi:10.1016/j.ydbio.2010.01.022

to the dorsal half of the neural tube, while dorsal midline regulators, such as BMP4, promote their dorsal expression at early steps of neural patterning (Goulding et al., 1994a; Liem et al., 1997; McMahon et al., 1998; Monsoro-Burq et al., 1995; Monsoro-Burq et al., 1996). In turn, Pax3 is an essential regulator of neural tube dorsal–ventral patterning. Splotch mutants are strongly affected in dorsal neural tube development and present severe spina bifida (Borycki et al., 1999; Epstein et al., 1991). Reciprocally, Pax3 gain of function in mouse embryos alters ventral neural tube patterning (Tremblay et al., 1996). Strikingly, the Pax7 homozygous mutants do not show any abnormal phenotype in the central nervous system, suggesting a significant functional overlap between Pax3 and Pax7 activities within the neural tube of mouse embryos (Mansouri et al., 1996). Indeed, *Pax7* knock-in into the *Pax3* locus in Splotch mutants rescues the spina bifida phenotype (Relaix et al., 2004). At later stages of brain morphogenesis, in chick embryos, *Pax3* and *Pax7* expression is regulated at the isthmus by Fgf8 and En2/Pax2–5; in turn, Pax3 and Pax7 are involved in tectum organisation downstream of Fgf8/En2/Pax2–5 (Matsunaga et al., 2001). During later mouse mesencephalon development, Pax3 and Pax7 expression partially segregate and control the development of specific neuronal populations (Thompson et al., 2008).

Pax3 and Pax7 are also major regulators of neural crest early development. The neural crest is a transient vertebrate-specific population of pluripotent and migratory progenitors, from which are derived peripheral neurons and glia, melanocytes and other pigment cells, as well as craniofacial structures (Le Douarin and Kalcheim, 1999). The neural crest delaminates from the dorsalmost part of the neural tube, after being induced in the lateral neural plate (also named the neural border, (Meulemans and Bronner-Fraser, 2004) during gastrulation and early neurulation. Mutations in the human Pax3 gene, which can be heterozygous or rarely homozygous, affect a subset of neural crest derivatives, such as the melanocytes, which, in particular, contribute to ear development and to pigmentation of skin and hair (Waardenburg syndrome I and III), but initial neural crest development seems to occur normally since other neural crest structures are formed (Read and Newton, 1997). In the mouse, homozygous Pax3 mutants display reduced to absent neural crest derivatives, especially in posterior areas, while heterozygous mice only show reduced belly pigmentation (Auerbach, 1954; Franz and Kothary, 1993; Relaix et al., 2004). Strikingly, the craniofacial structures form rather normally in Pax3 homozygotes, suggesting that the initiation of neural crest development is not affected in the cephalic neural crest (Relaix et al., 2004). Mouse Pax7 mutants show only late cephalic neural crest defects (Mansouri et al., 1996), suggesting that Pax3 activity is sufficient for early neural crest. Overlap between Pax3 and Pax7 functions in the neural tube and neural crest is further evidenced by the rescue of the Pax3 mutant phenotype by knock-in of Pax7 into the Pax3 locus, showing that increasing Pax7 activity compensates for Pax3 loss (Relaix et al., 2004). Because of the overlapping expression and roles, and because the double mutant Pax3/Pax7 has not yet been described, the contributions of Pax3 or Pax7 to mammalian cranial neural crest induction remain unknown. However, in non-mammalian species, both Pax3 and Pax7 have been implicated in neural crest induction. In particular, *Pax3* appears as the earliest neural border-specific marker in the *Xenopus laevis* gastrula (Monsoro-Burq et al., 2005), a similar pattern being assumed by *Pax7* in chick embryos (Basch et al., 2006). In either species, Pax3 (*Xenopus*) or Pax7 (chick) cooperate with other regulators and induce the early neural crest marker *Snail2* (Basch et al., 2006; Monsoro-Burq et al., 2005). By contrast, the respective roles of *Xenopus* Pax7 and chick Pax3 in neural crest induction remain to be explored. Moreover, besides interactions between the neural plate and the ectoderm, interactions between the paraxial mesoderm and the ectoderm are essential in neural crest induction (Bonstein et al., 1998; Monsoro-Burq et al., 2003). Although Pax3 and Pax7 are important regulators of paraxial mesoderm development (Borycki et al., 1999; Goulding et al., 1994b; Relaix et al., 2004, 2005), their potential participation in the neural crest inducing activity of the paraxial mesoderm remains to be explored.

During later neural crest development, Pax3 and Pax7 are found in migrating neural crest cells (NCC) with species-specific differences: cranial NCC in mouse, cranial and trunk NCC in chick and zebrafish embryos (Lacosta et al., 2005; Mansouri et al., 1996; Minchin and Hughes, 2008). When NCC condense into dorsal root ganglia in chick embryos, *Pax3* remains expressed while *Pax7* expression is extinguished (Lacosta et al., 2005). Later, both *Pax3* and *Pax7* are detected in the neural crest derived pigment cells, melanocytes or xanthophores in chick or zebrafish (Lacosta et al., 2005; Minchin and Hughes, 2008). However, only *Pax3* was detected in mammalian melanoblasts (Lacosta et al., 2005). In conclusion, the survey of Pax3 and Pax7 expression profiles in various vertebrates outlines the variability of common and gene-specific patterns, especially in the neural crest lineage.

In this study, we have examined and compared the respective roles of Pax3 and Pax7 in neural and neural crest patterning in *Xenopus* embryos. We show striking differences in the expression domains of these two genes compared to other vertebrate species, notably in the neural tube and neural crest, that could indicate different functional specialization between the two genes in amphibians. Using a series of gain-of-function and loss of function experiments, we address the regulation of Pax7 expression by FGF, Wnt, retinoids and Pax3 during early neural patterning. We then analyze and compare Pax3 and Pax7 specific function in early anterior–posterior brain patterning. Finally, we explore their respective roles in neural crest induction by the paraxial mesoderm.

Materials and methods

Embryo and explant manipulation

X. laevis embryos were obtained by in vitro fertilization using standard procedures and were staged according to Nieuwkoop and Faber developmental table (Nieuwkoop and Faber, 1994; Sive et al., 2000). Embryos were injected in one blastomere at the two to four-cell stage unless otherwise noted. Co-injection of mRNA encoding nuclear-targeted *lacZ* traced the progeny of the injected blastomere. Staining for beta-galactosidase activity was done prior to final fixation (Monsoro-Burq, 2007). The recombination of stage 9 ectoderm from the animal cap to stage 10.25 prospective paraxial mesoderm (dorsal–lateral marginal zone, DLMZ), as an assay for neural crest induction, was described in Bonstein et al. (1998) and Monsoro-Burq et al. (2003).

Semi-quantitative RT-PCR

Embryos were lysed in proteinase K-containing lysis buffer, followed by DNase treatment and reverse transcription (Sive et al., 2000), the minus-RT sample is a control sample amplified without the reverse transcription step, monitoring potential DNA contamination. *EF1a* was used to calibrate the reaction (21 cycles, Krieg et al., 1989). *Muscle actin*, *snail2*, *vent1*, *myod*, *pax3* and *pax7* primers (Mizuseki et al., 1998; Monsoro-Burq et al., 2005; Rupp and Weintraub, 1991; Shapira et al., 1999; Stutz and Spohr, 1986, and this study) were used in 25-cycle amplification ^{32}P-dCTP-traced PCR (see Supplemental Fig. 2A for sequences).

Whole mount in situ hybridization (ISH) and immunostaining

Embryos were fixed and prepared for whole mount in situ hybridization (ISH) according to a shortened protocol optimized for superficial structures (Monsoro-Burq, 2007). Antisense digoxigenin-labelled RNA probes were used at a final concentration of 1 μg/ml.

Probes were described elsewhere: *snail2* (Grammer et al., 2000), *pax3* (Monsoro-Burq et al., 2005), *myoD* (Hopwood et al., 1989), *otx2* (Lamb et al., 1993), *en2* (Hemmati-Brivanlou et al., 1991), *krox20* (Bradley et al., 1993), *gbx2* (PCR-amplified and cloned into pGEM-T Easy (Promega) using sequence in Tour et al. (2002a)), *dct* (Kumasaka et al., 2003) and *hoxb9* (Sharpe et al., 1987). For immunostaining of myotome after ISH, the bleached embryos were saturated in 10% serum then incubated in 12/101 monoclonal antibody (Kintner and Brockes, 1984) before washes and peroxidase (HRP-DAB) staining. The embryos were examined after vibratome (30 µm) sectioning.

Messenger RNA synthesis, antisense morpholinos

Messenger RNAs used for microinjection were obtained by in vitro transcription of plasmids containing the desired cDNA using the mMessage mMachine SP6 or T7 kits (Ambion) and purified on G50 sephadex spin columns. The following plasmids were used: *nlacZ* (125–250 pg/cell), *fgf8a* (CS107-*fgf8a*;10–50 pg/cell) (Monsoro-Burq et al., 2003), *wnt7b* (50 pg/cell) (Chang and Hemmati-Brivanlou, 1998; Grammer et al., 2000), *dnRARα* (250 pg/cell) (Blumberg et al., 1997), *X. laevis pax3* (AY725269; cloned into CS107-*Pax3*, 125 pg/cell) (Monsoro-Burq et al., 2005), mouse *pax3* (CS107-*mpax3*, 125 pg/cell) (Goulding et al., 1991; Monsoro-Burq et al., 2005), mouse *pax3-EnR* (subcloned into pCS107 by R. Harland and B. Martin, 62–125 pg/cell; Ridgeway and Skerjanc, 2001), *X. laevis pax7* (full-length cDNA subcloned into pCS107, 250–500 pg/cell, this study, Genbank AY725267), *X. laevis pax7-myc* (*pax7* ORF fused to N-terminal myc tags and subcloned into pCS107, 62–125 pg/cell, this study), *X. laevis pax7-EnR* (pCDNA3-*pax7-EnR*, *pax7* DNA binding domain fused to Engrailed repressor domain, 62 pg/cell (Chen et al., 2006). Silencing of selected genes was performed using translation blocking antisense morpholino oligonucleotides (GeneTools, see Supplemental Fig. 2B for sequences): Fgf8MO (Monsoro-Burq et al., 2003), beta-cateninMO (Genetools), Pax3MO (Monsoro-Burq et al., 2005), Pax7MO (translation blocking), Pax7 mismatch MO and Pax7 splice MO (this study). The specificity of Pax3MO and Pax7MO (translation blocking MOs) MOs was tested by ^{35}S-labelled in vitro transcription-and-translation reaction using TNT kit (Promega). Relative morpholino concentration was maintained constant compared to the volume of the injected cell: whole embryo injections were done in all blastomeres at the two or four-cell stage with a total dose four times higher than injections done into one blastomere of four-cell stage embryos.

Results

pax3 and pax7 display both partially overlapping and distinct expression domains in mesoderm, neural plate and brain of X. laevis embryos

We previously subcloned and sequenced the full-length *pax7* cDNA from NIBB EST library (http://xenopus.nibb.ac.jp, Genbank accession #AY725267). As expected, the encoded protein shows high similarity with other vertebrate Pax7 especially within the paired and octapeptide-homeodomain parts of the protein (Supplemental Figs. 1A–B) and synteny in *Xenopus tropicalis* (not shown). In contrast, Pax3 and Pax7 proteins, although very closely related, can be clearly distinguished by several amino acid sequence features and are quite distinct at the nucleotide level (Supplemental Figs. 1C and 2C), allowing construction of a non-ambiguous phylogenetic tree. We have analyzed the available Pax3/7 sequences in chordates, using neighbour-joining method (Clustal W in MacVector and MEGA4 software (Tamura et al., 2007). This tree groups the cyclostomes (lamprey and hagfish) genes in the Pax7 group, while both amphioxus and ascidian are found with a single Pax3/7 gene. This confirms that the duplication of the Pax3/7 ancestor has occurred at the base of the vertebrate lineage (Fig. 1A; O'Neill et al., 2007). Moreover, we have also compiled the available data on Pax7 gene organisation using both *X. laevis* BAC sequencing and *X. tropicalis* genome data (Supplemental Fig. 2).

We compared the onset of *pax3*, *muscle actin*, and *pax7* transcription in vivo using semi-quantitative RT-PCR on whole embryos (Fig. 1B). As we described before, *pax3* appears the earliest, at gastrula stage 11 (Monsoro-Burq et al., 2005), followed by *muscle actin* which is detected by stage 12.5. *Pax7* appears last, being faintly detected at mid-neurula stage 14, then being reinforced in tadpoles (from stage 26 onwards). We have further compared expression patterns of *pax3*, *pax7*, *snail2* and *myoD* by whole mount ISH, at neurula stages. In agreement with the RT-PCR data, we found that *pax7* is faintly expressed by stage 14 in the anterior neural plate (Fig. 1C, a, c) and reinforced in the brain and trunk paraxial mesoderm by stage 18 (Fig. 1C, b, d). This expression is thus detected at a later developmental stage than *pax3* (detected at the neural border at stage 14 and in neural plate and paraxial mesoderm later on, Fig. 1C, e, f), *snail2* (detected in the neural crest at both stages 14 and 18, Fig. 1C, g, h) and *myoD* (expressed in the entire paraxial mesoderm at stages 14 and 18, Fig. 1C, i, j).

At tailbud stage, *pax3* and *pax7* remain expressed in overlapping but distinct domains in both neural tissue and somites. At stage 23, a strong *pax7* staining is observed in the posterior part of the brain and in the paraxial mesoderm (Figs. 2A–B, D–E). This pattern differs from *pax3* expression, which extends the entire length of the nervous system (Figs. 2C, F). In addition, *pax3* stains the hatching gland in the ectoderm (Fig. 2C). Double staining with *krox20* helps define the *pax7*-positive brain level: *pax7* is expressed in a domain centered on rhombomeres 3 and 5 (Figs. 2G–H, J–K, yellow arrows), including mesencephalon and anterior spinal cord while *pax3* labels the entire length of the neural tube (Figs. 2I, L). Transverse trunk sections (line in Fig. 2J), double-stained with 12–101 muscle marker show that *pax7* labels the superficial part of the myotome as well as a dorsal spinal cord domain excluding the roof plate, while *pax3* labels the hypaxial myotome and the entire dorsal domain of the spinal cord (Figs. 2M–O). Since the origins of the dermatome are unclear at this stage, we cannot rule out a contribution of gene expression to this domain. Neither of the two genes is expressed in the migrating neural crest (compare to *krox20*-positive neural crest from rhombomere 5 in Figs. 2K–L).

Both pax7 and pax3 respond to FGF, WNT and retinoic acid pathways patterning activity

The differences observed in the expression of *pax7* and *pax3* might result from the cues that define the anterior–posterior neural pattern in the neurula embryos. During neural development, FGF signaling contributes to neural induction and anterior–posterior polarization of the neural tube (Delaune et al., 2005; Fletcher et al., 2006). Moreover, FGF8 is a major brain patterning signal at the midbrain–hindbrain boundary (Koebernick et al., 2006). FGF8 expression is first detected at this boundary by stage 16 in *X. laevis* neurulae, which is similar to the observed onset time of *pax7* expression in the brain (Fig. 1C).

We analyzed the role of FGF signaling on *pax7* patterning by gain and loss of function experiments. *Fgf8a* mRNA injections were done in one dorso-animal blastomere at the 4-cell stage, at a low dose (5 pg) that only marginally affects gene expression on the contralateral side as monitored by *snail2* expression ($n=8$, 75% of unilateral expansion of *snail2* at stage 18, 12% expansion in the anterior neural fold, not shown, (Monsoro-Burq et al., 2003). Increased FGF8 signaling resulted in expanded *pax7* expression: at neurula stage 18, the anteriormost expression domain, located in the prospective forebrain was lost while the emerging rhombencephalon domain and the mesoderm domain were shifted anteriorly (black arrows) (Fig. 3A). At tailbud stage (stages 20–25), *pax7* was found expressed in the whole brain on the injected side, extending anteriorly towards the forebrain ($n=31$, 84% expansion, Fig. 3C, arrow). Interestingly, the posterior boundary of *pax7* expression in the rhombencephalon remained unchanged. In

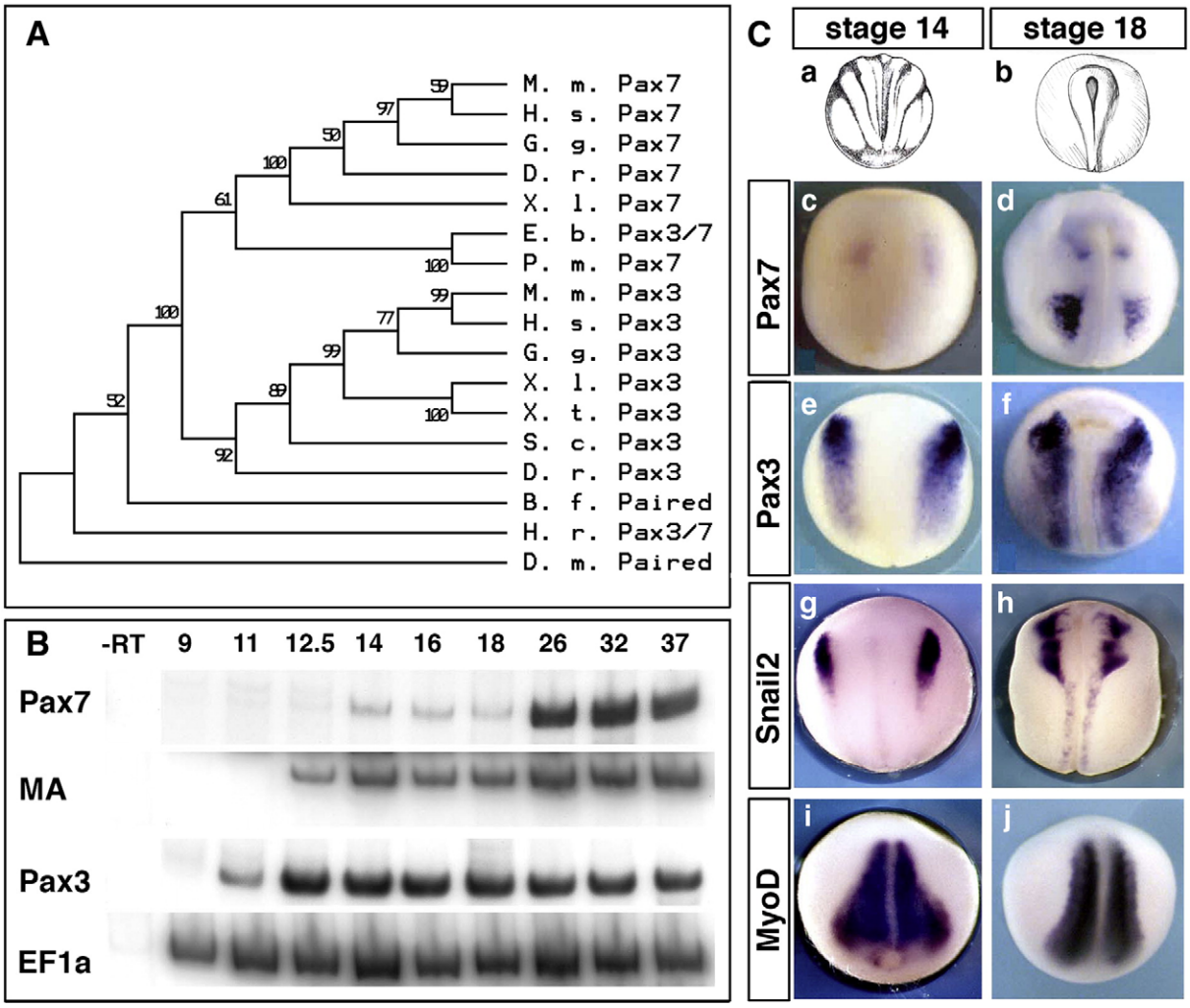

Fig. 1. Expression of *pax7* and *pax3* compared during neurulation in *Xenopus laevis*. (A) A bootstrap phylogenetic tree illustrates the clear grouping of *pax7* and *pax3* paralogs in vertebrates while the chordate have a single Pax3/7 gene. Accession numbers are given in Supplemental Fig. 1. (B) RT-PCR analysis on whole embryos shows the early onset of *pax3* expression during gastrulation (i.e. at times of neural crest induction), whereas *pax7* is detected at mid-neurulation, after *muscle actin* (*MA*) is detected. *EF1α* is used as a baseline control. (C) In situ hybridization on stage-matched sibling embryos confirms the late onset of *pax7*, in brain first (c) then in paraxial mesoderm, and the lack of expression in the neural crest progenitor area (c, d). In contrast, *pax3* and *snail2* label neural crest (e–h). *Myod* marks paraxial mesoderm (i, j).

sibling embryos, FGF8 over-expression enlarged *pax3* expression domain in the dorsal neural tube ($n=27$, 100% expansion, not shown, (Monsoro-Burq et al., 2005)) as well as *krox20* expression in rhombomeres 3 and 5 ($n=24$, 83% expanded, not shown). Conversely, knocking down both FGF8a and FGF8b forms by a translation blocking morpholino against *X. laevis* FGF8 (FGF8MO, (Fletcher et al., 2006; Monsoro-Burq et al., 2005), Supplemental Fig. 2B) efficiently downregulated both *pax7* and *pax3* expression in the brain on the injected side (*Pax7*: $n=20$, 85% decrease to complete loss of expression, Figs. 3B, D; *Pax3*: $n=10$, 60% decrease, not shown). This was similar to the decrease observed after injection of a dominant-negative FGF receptor (XFD, not shown). This result shows that FGF signaling, and FGF8 in particular, play an essential part in initiating and patterning *pax7* expression in the brain.

We have then asked at what time of neural patterning were FGF signals required to establish a proper *pax7* pattern in the brain: either as part of the general neural anterior–posterior patterning or more specifically during isthmus formation. We blocked FGF signaling using the FGF receptor inhibitor SU5402 during three periods of development, in three groups of sibling embryos: group 1 was treated from late blastula to early tadpole stage (from stages 8 to 22), group 2 during neural induction only (from stages 8 to 12) and group 3 during neural patterning (from stages 12 to 22) (Delaune et al., 2005). The first two treatments inhibit neural induction and mesoderm formation as noted by the reduced *sox2* expression (100% reduction, $n=21$; DMSO treated sibling are 92% normal, $n=24$) and the severe gastrulation defects observed in these embryos. The third treatment avoids perturbing general mesoderm and neural induction as shown by *sox2* expression analysis: 96% of the embryos show normal *sox2* staining ($n=23$) while 100% of DMSO treated siblings are normal ($n=22$). However, this treatment alters posteriorization of the neural plate as marked by decreased *hoxb9* expression (Supplemental Fig. 3, $n=23$, 61% decreased expression; DMSO treated siblings are 100% normal ($n=22$); Fletcher and Harland, 2008; Roche et al., 2009). In all cases, *pax7* expression was analyzed at stage 22. For all three periods of treatment, we observed *pax7* expression in the brain in the majority of the embryos. There was an altered *pax7* pattern in the anteriormost part of the nervous system that still forms when embryos are treated early (treatments done between stages 8–12 (group 1) and 8–22 (group 2): $n=24$, 71% of embryos showed slightly reduced to normal staining, 29% had a loss of staining, compared to DMSO treated siblings ($n=23$, 100% normal staining) (data not shown). This reduction correlated with the abnormal *sox2* expression. There was no significant loss of *pax7* expression in group-3 embryos: normal expression was observed in the majority of both in DMSO treated embryos, ($n=23$, 100% normal) and SU-treated

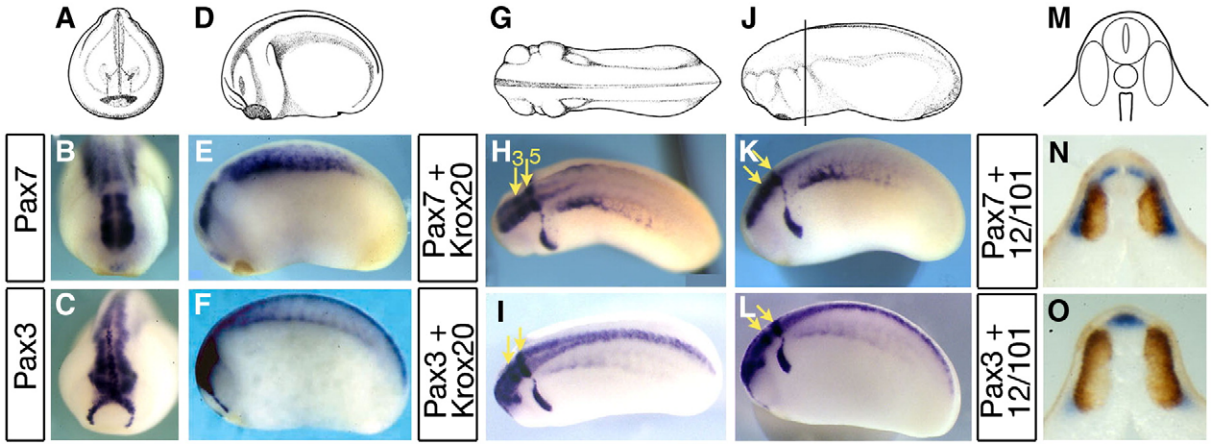

Fig. 2. Distinct *pax7* and *pax3* patterns in central nervous system and paraxial mesoderm at tailbud stages. (A–C) Front views of stage 22 embryos (A) show *pax7* expression in the caudal part of the brain (B), whereas *pax3* labels both the whole brain and the hatching gland (C). (D–F) Side views (D) illustrate *pax7* restriction to mesencephalon, hindbrain and anterior spinal cord whereas *pax3* is found along the entire anterior–posterior length of the central nervous system. *Pax7* labels the central paraxial mesoderm while *pax3* is found in hypaxial cells. (G–L) Dorsal (G–I) and side (J–L) views of tailbud stage 24, with double staining for *pax3* or *pax7* and *krox20*, which labels hindbrain rhombomeres r3 and r5 (yellow arrows), confirms the limited extent of *pax7* expression along the spinal cord. (M–O) Tailbud stage 24 transverse sections were double-stained with 12–101 myotome marker (brown). This shows *pax7* expression in the alar plate of the anterior-most spinal cord and medial myotome (N) and *pax3* in the roof plate, alar plates and in the hypaxial myotome (O).

embryos ($n=35$, 60% with normal staining and 31% with a moderate decrease in the extent of *Pax7* domain and staining intensity (see Supplemental Fig. 3). This result indicates that FGF signaling plays a major role in regulating *pax7* expression during early brain patterning but only marginally modulates *pax7* pattern at later neurulation stages such as during isthmus formation.

Additionally, FGFs cooperate with Wnt and Retinoic acid signals to pattern the midbrain and hindbrain (Blumberg et al., 1997; McGrew et al., 1997). We have either over-expressed Wnt7b or injected a beta-catenin morpholino to activate or block the Wnt-beta-catenin pathway respectively. As observed for FGF signals, an increased Wnt signaling resulted in an enlarged *pax7* expression domain ($n=20$, 65% increase, Fig. 3E), with a posterior border shift, similar to what is observed for *pax3* in sibling embryos ($n=13$, 77% increased; not shown, (Monsoro-Burq et al., 2005)). Conversely, *pax7* expression was strongly decreased to absent in beta-catenin morpholino-injected embryos ($n=35$, 77% decrease, Fig. 3F). Retinoic acid signaling was blocked using a dominant-negative form of retinoic acid receptor alpha (dnRARα, Blumberg et al., 1997), resulting in decreased *pax7* expression in the injected area ($n=13$, 70% decrease, Fig. 3G). Together, these results show that the three main posterior neural patterning pathways, namely FGF, Wnt and RA, are active in defining the *pax7*-positive domain; that they act during early neurulation rather than mid–hindbrain boundary formation, and that the differences observed between *pax3* and *pax7* domains in *X. laevis* are not due to a loss of competence to respond to these patterning cues in *pax7* gene regulatory elements.

Pax3 regulates pax7 expression in the brain

Focusing on neural patterning, we next asked if Pax3, which is expressed earlier and in a larger domain that *pax7* in neural tissue, was involved in *pax7* patterning. In order to analyze the regulation of *pax7* expression by Pax3, we used an antisense morpholino-mediated depletion of Pax3 in conjunction with a rescue experiment (Monsoro-Burq et al., 2005). Using an in vitro reticulocyte lysate transcription-coupled-to-translation assay, we have first verified that Pax3MO efficiently and specifically blocked the translation of *X. laevis Pax3* cDNA (Fig. 4A, lanes 1–3), while it affected neither the translation of mouse *Pax3* cDNA (Fig. 4A, lane 4), nor that of the Pax7 cDNA (see Supplemental Fig. 2C and below Fig. 6A, lane 5).

In vivo, *pax7* expression is strongly decreased by Pax3 knock-down (20–30 ng) in the brain, analyzed at stages 22–25, while the contralateral side remains unaffected (81%, $n=106$) (Fig. 4C). This inhibitory effect is rescued when a moderate amount of mouse *pax3* mRNA (100 pg), insensitive to the Pax3MO, used is co-injected with Pax3MO (30 ng): in experimental series where Pax3MO-injected embryos showed a 90% loss of *pax7* ($n=25$) and expression in only 10% of the embryos, the sibling group, co-injected with Pax3MO and mouse *pax3* mRNA, displayed restored *pax7* expression in 46% of the embryos while 54% still showed decreased *pax7* expression ($n=39$) (Fig. 4B). We then analyzed the phenotype of Pax3-depleted embryos on transverse sections to evaluate the extent of loss of *pax7* expression in the dorsal–ventral neural axis. Compared to the normal situation (Fig. 4F) and to the contralateral side (Fig. 4G), the size of the dorsal brain domain is reduced and *pax7* expression strongly impaired (Fig. 4G). A very similar phenotype was obtained by injecting a repressor form of Pax3 (Pax3-engrailed repressor domain fusion; Ridgeway and Skerjanc, 2001): *pax7* expression was decreased both in wholemount views and on transverse sections, accompanied by a reduced size of the alar plate on the injected side ($n=21$, 95% decrease, Figs. 4D, H). The loss of *pax7* expression seems independent from a potential mechanical or indirect effect due to the spina bifida phenotype caused by Pax3MO or Pax3EnR since some embryos with severe spina bifida still displayed Pax7 staining on the non-injected side, while the expression was lost in the injected cells (not shown).

We next examined the effect of increasing Pax3 activity in vivo by injection of *Xenopus* or mouse mRNA around the prospective neural plate (250 pg into one dorsal animal blastomere at 4-cell stage). A clear expansion of *pax7* expression is observed in about half of the injected embryos (54% expansion, $n=94$ Fig. 4E), which is rather modest when compared to sibling embryos analyzed for *Snail2* expression as a positive control (69% expansion, $n=54$, not shown). A similar effect was obtained using mouse *Pax3* mRNA (expansion in 8 embryos out of 13, not shown). On transverse sections, it appeared that the expansion is due to an enlargement of the alar plates, accompanied by the expansion of *pax7* expression dorsally (Fig. 4I). The sum of these observations suggest that Pax3 regulates general alar plate patterning, acts as an activator in *pax7* regulation and is required for *pax7* induction and patterning in the brain.

Pax7 is expressed later, in brain, myotome, lymph heart and melanocytes

In tadpole stage embryos, *pax7* is expressed in four main locations: the brain, the superficial part of the somite, the lymph heart and the

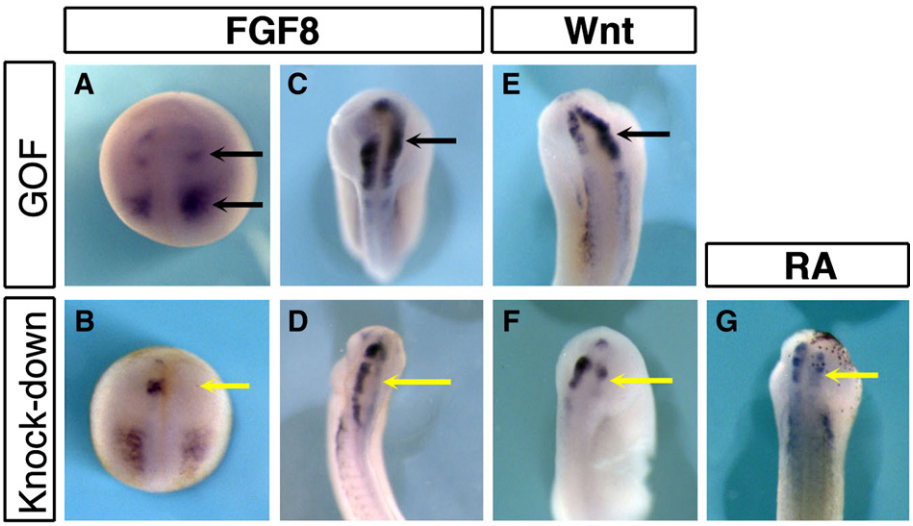

Fig. 3. *pax7* pattern in the brain is positively regulated by FGF, Wnt and retinoid signals. (A–D) FGF8 gain of function expands *pax7* expression into forebrain, while FGF8 depletion leads to lack of *pax7* at induction stage (stage18, A, B) and in later development (stage 22, C, D). (E–F) *Wnt7b* over-expression and beta-catenin morpholino injections demonstrate the requirement for Wnt signals in *pax7* patterning. (G) Similarly, blocking retinoic acid signaling resulted in defective *pax7* expression.

melanocytes. As observed at earlier stage, at stage 25, *pax7* is restricted to midbrain, hindbrain and the most anterior part of the spinal cord, contrasting to *pax3* expression that extends along the entire neuraxis (Fig. 5A/A,E, red arrows). In the paraxial mesoderm, both *pax7* and *pax3* are found with patterns similar to those of stage 22 embryos (Figs. 2 and 5A/A,E, compare to *myoD* staining in I). At later stages (stage 32 onwards), a similar *pax7* brain expression is observed, as well as a faint more posterior spinal cord staining (Fig. 5A/B,F). While *pax3* marks the trigeminal ganglia (Fig. 5A/F, arrow), *pax7* expression is not observed at this location but is found in the lymph heart (Ny et al., 2005), (Fig. 5A/B, arrow). At this stage, *pax7* expression is no longer detected in the paraxial mesoderm (Fig. 5A/B) while *pax3* still strongly labels the hypaxial muscle and intersomitic areas (Fig. 5A/F, compare to *myoD* in Fig. 5A/J) (Martin and Harland, 2001). We have further documented *pax7* expression in the lymph heart by comparing it to lymph heart marker *prox1* expression in stage-matched sibling embryos: we found that *pax7* is expressed earlier than *prox1*, but both genes are expressed later (Fig. 5B/A–D). At swimming tadpole stage 41, *pax7* is found in a dispersed population of cells in the body wall, while *pax3* is found at the edge of the migrating paraxial muscle progenitors (Fig. 5A/C, G, yellow arrows, compare to *myoD* staining in Fig. 5A/K). *Pax7* is detected again in the myotome, in cells that align at the edge of each myotome (Fig. 5D). We propose that these cells may constitute the future satellite cell population described in mature muscles (Chen et al., 2006). At stage 45, *pax7* and *pax3* are both expressed in the melanocytes (Fig. 5A/D, H). We have analyzed the co-localisation of *pax7* expression with eumelanin by comparing pictures of the same embryos, taken either before bleaching or after in situ staining (Fig. 5C). While neither *myoD* nor *prox1* — (used here as bleaching and in situ hybridization control) stain these cells (Fig. 5A/L), there is a striking co-localisation of *pax7* staining and melanosomes (Fig. 5C/A,B, arrows).

Pax7 loss of function affects brain, muscle and melanocyte development

We have designed a Pax7-specific translation blocking antisense morpholino oligonucleotide that has no complementarity to Pax3 cDNA sequence (Supplemental Fig. 2F). We have checked using in vitro transcription–translation reticulocyte lysate assay, that Pax7MO efficiently blocks *Pax7* translation (Fig. 6A, lanes 1–3), but not translation from a construct lacking the MO complementary sequence (Pax7-myc-GFP fusion, Fig. 6A, lane 4) nor from a Pax3 construct (Fig. 4A, lane 5). Pax3MO did not block Pax7 translation either (Fig. 6A, lane 5). Embryos were injected bilaterally with either control, Pax7MO or Pax3MO. Until early-mid-neurula stages (stage 14), embryos injected with either Pax7MO (70 ng) or Pax3MO (70–80 ng) did not exhibit obvious morphological defects compared to sibling embryos (data not shown). This indicates that gastrulation and neurulation initiate normally, consistent with the lack of Pax7 expression at these stages. At late neurula and tadpole stages, three main phenotypes were observed after Pax7MO bilateral injection in vivo: head atrophy, shortened axis with (posterior) spina bifida and melanocyte loss. These phenotypes were compared to that of control and Pax3MO-injected siblings, which also display spina bifida and loss of melanocytes, but less severe head malformation (Fig. 6). The majority of the Pax7MO-injected tadpoles did not close the neural tube and exhibited a shortened axis with mild (brain is closed, 10.3%, $n=398$, Fig. 6D, f) to severe spina bifida (87.4%, $n=398$) (Fig. 6D, k). When embryos that exhibit severe spina bifida developed further, they died between stages 24 and 26 (i.e. too early for melanocyte lineage analysis). The embryos with less severe neural defects survived until stages 33–40, provided that the vitelline envelope was manually removed (Fig. 6D, g–j and l–o, $n=38$): these latter embryos showed severely altered anterior morphology, with reduced head, reduced eyes and few/no melanocytes (severe melanocyte loss, with no lateral migration, 81%, $n=38$). A similar phenotype was observed when a Pax7-EnR fusion was injected bilaterally (not shown).

At stage 23, Pax3 morphants were fairly normal, although cell death dorsal to the neural tube was observed (not shown), suggesting that unspecified neural crest cells die at the end of neurulation (Monsoro-Burq et al., 2005). These embryos did not hatch autonomously and were devitellinized manually around tailbud stages 22–23. At stages 26–33, Pax3MO-injections resulted in a shorter body axis than normal but more elongated than Pax7 morphants (Fig. 6D, q, v). In addition, head and fin defects were prominent, spina bifida was frequently observed especially in the posterior neural tube (18%, $n=162$) (Fig. 6D, p–r and u–w). Those features mimic the Splotch mutant phenotype (Auerbach, 1954; Epstein et al., 1991).

We have used embryos displaying the milder phenotype to assess muscle and pigment formation at tadpole stage by ISH. Stage 26–33 Pax7 morphants showed *myoD* staining only in a reduced posterior area (Fig. 6D, j, o), while Pax3MO injections resulted in a rather normally elongated *myoD* area along the side of the embryo (Fig. 6D, t, y), although the segmentation pattern was severely altered (Supplemental Fig. 4). Melanocyte differentiation was assessed in stage 26–40 embryos using either *dct* staining for melanocyte precursors (Fig. 6D) or

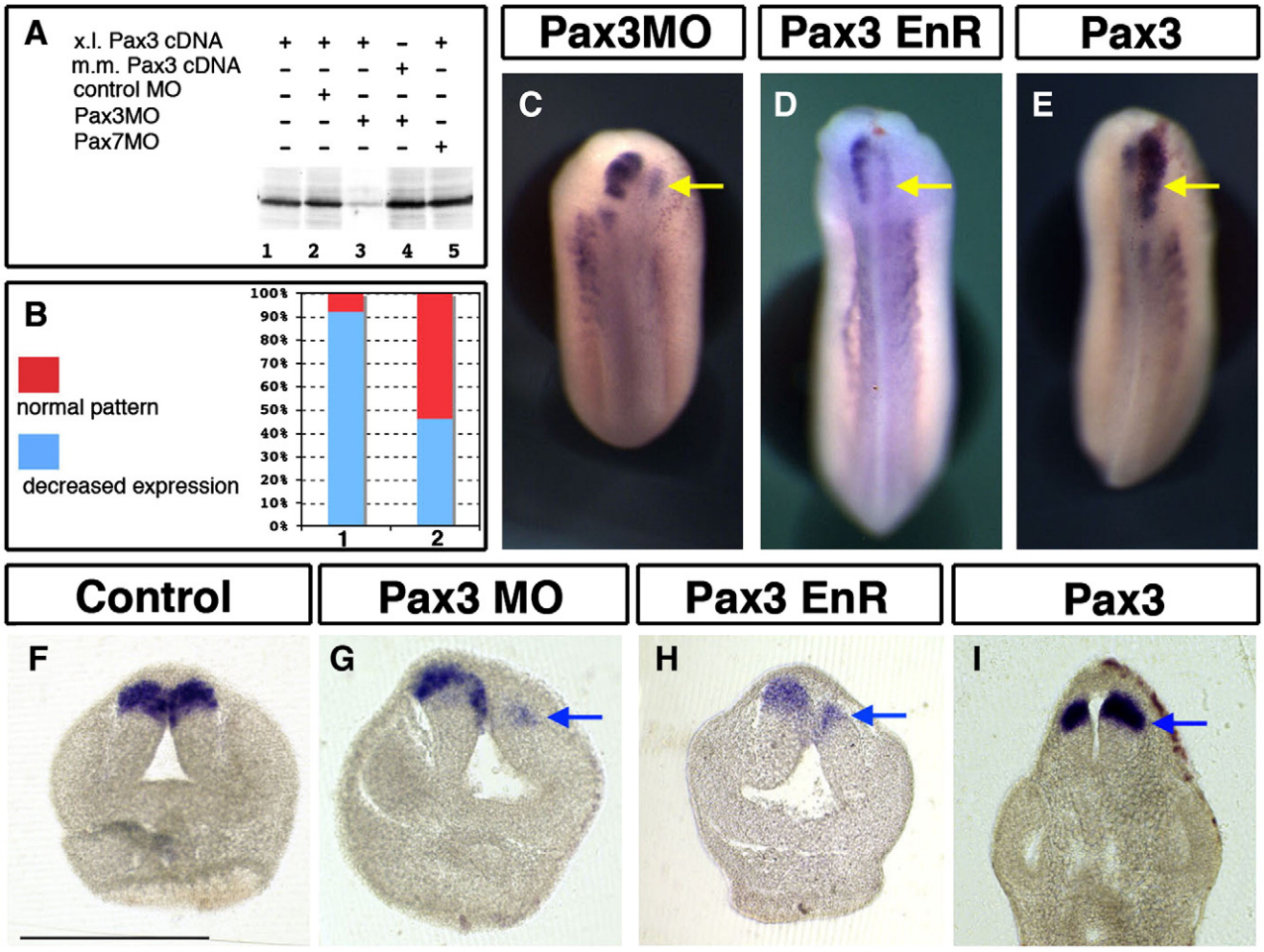

Fig. 4. Pax3 regulates *pax7* expression and alar plate patterning in the brain. (A) Pax3 depletion using an antisense morpholino (Pax3MO) specifically prevents *Xenopus laevis pax3* translation in vitro (lane 3). Pax7MO and a control MO have no effect on *Xenopus laevis pax3* translation while *Mus musculus pax3* is unaffected by Pax3MO. (B) Following Pax3 depletion in vivo (bar 1), *pax7* expression is severely reduced, *Mus musculus Pax3* mRNA efficiently rescues the decrease in *pax7* expression (bar 2). (C) Unilateral depletion of Pax3 results in loss in *pax7* expression; (D) a similar effect is observed after Pax3-EnR over-expression. (E) Gain in Pax3 activity increases and expands *pax7* expression. (F–I) Transverse sections show that the loss in *pax7* (C, D, G, H) is accompanied by reduced alar plates development, while Pax3 increase results in expanded *pax7*-expressing alar plates (I). Bar = 500 µm.

eumelanin pigment as a marker in lightly pigmented eggs or albino eggs fertilized with sperm from a pigmented male (not shown). Pax7 morphants lacked *dct* expression (81.6%, $n = 38$, Fig. 6D, h, m and i, n, compare to stage-matched control in Fig. 6D, c, d). Similarly, the number of melanocytes in Pax3MO-injected embryos was either reduced (i.e. some melanocytes are observed dorsal to the neural tube, but very few melanocytes have migrated laterally, 30%, $n = 103$ Fig. 6H) to severely depleted (no melanocyte observed, Fig. 6O, 40%, $n = 103$, compared to stage-matched control in Fig. 6D, c, d). Together, these observations suggest that head and brain development, muscle and neural crest derivative formation are affected by the depletion of Pax7 and Pax3 activity in vivo. However, the phenotypes observed present clear gene-specific features.

To address the specificity of this phenotype, we have rescued the Pax7MO phenotype by co-injecting the Pax7-myc fusion, insensitive to the MO. Embryos injected with Pax7MO exhibit the defects described above on the injected side at the end of neurulation (stage 18, 54% of defective embryos, $n = 111$), but the sibling embryos co-injected with Pax7MO and Pax7-myc mRNA are fairly normal in 74% of cases, $n = 291$) (Fig. 6E). The rescued embryos also displayed rescued expression of *myoD* and *dct* (Fig. 6F). To further address the specificity of the observed phenotype, we have injected a morpholino with 5-mismatches compared to Pax7MO (see Supplemental Fig. 2C). In this case, both morphology of the embryos and gene expression were normal (Supplemental Fig. 5). Furthermore, we have designed a splice-blocking morpholino, preventing splicing of the first intron (Supplemental Fig. 2). In this case, we evaluated the level of *pax7* knock-down to 60% by semi-quantitative RT-PCR at stage 22, using embryos injected with the Pax7 splice MO in all four blastomeres (Supplemental Fig. 6A). Whole embryo injections resulted in a similar phenotype as described above for Pax7MO (although is a slightly lower proportion of the embryos with most severe phenotypes) and *snail2*, *myod* and *dct* expression were affected similarly (Supplemental Fig. 6).

Pax7 function is essential for neural crest formation

Since morphological alterations appear during neurulation, we examined if Pax7, like Pax3, is important in neural and neural crest development in *Xenopus*. We have analyzed the effects of Pax7 depletion on *krox20* expression, (*krox20* labels hindbrain rhombomeres 3 and 5, and neural crest emigrating from rhombomere 5, Fig. 7A) and on *snail2* expression (Fig. 7F) in stage 18 neurulae. *Krox20* expression was severely altered both in the brain and in the neural crest: rhombomere 3/5 staining was either shifted posteriorly or lost, while rhombomere 5 neural crest was diminished or lost (95%, $n = 61$; Figs. 7B, C). Similarly, *snail2* expression was strongly reduced or completely abolished on the injected side (74%, $n = 43$; Figs. 7G, H). Similar phenotypes were

observed with Pax7-EnR fusion (70%, $n=57$ for *krox20* and 69.7%, $n=76$ for *snail2*; Figs. 7D, I) and Pax3MO (75%, $n=45$ for *krox20* and 76% $n=47$ for *snail2*; Figs. 7E, J), suggesting redundant effects of Pax3 and Pax7 in this process.

To assess the specificity of Pax7 morpholino phenotype, we have performed a rescue experiment, using a *pax7-GFP-myc* fusion. Sibling embryos were injected unilaterally with either Pax7MO, or co-injected by Pax7MO and the *pax7-GFP-myc* mRNA (125 pg). Snail2

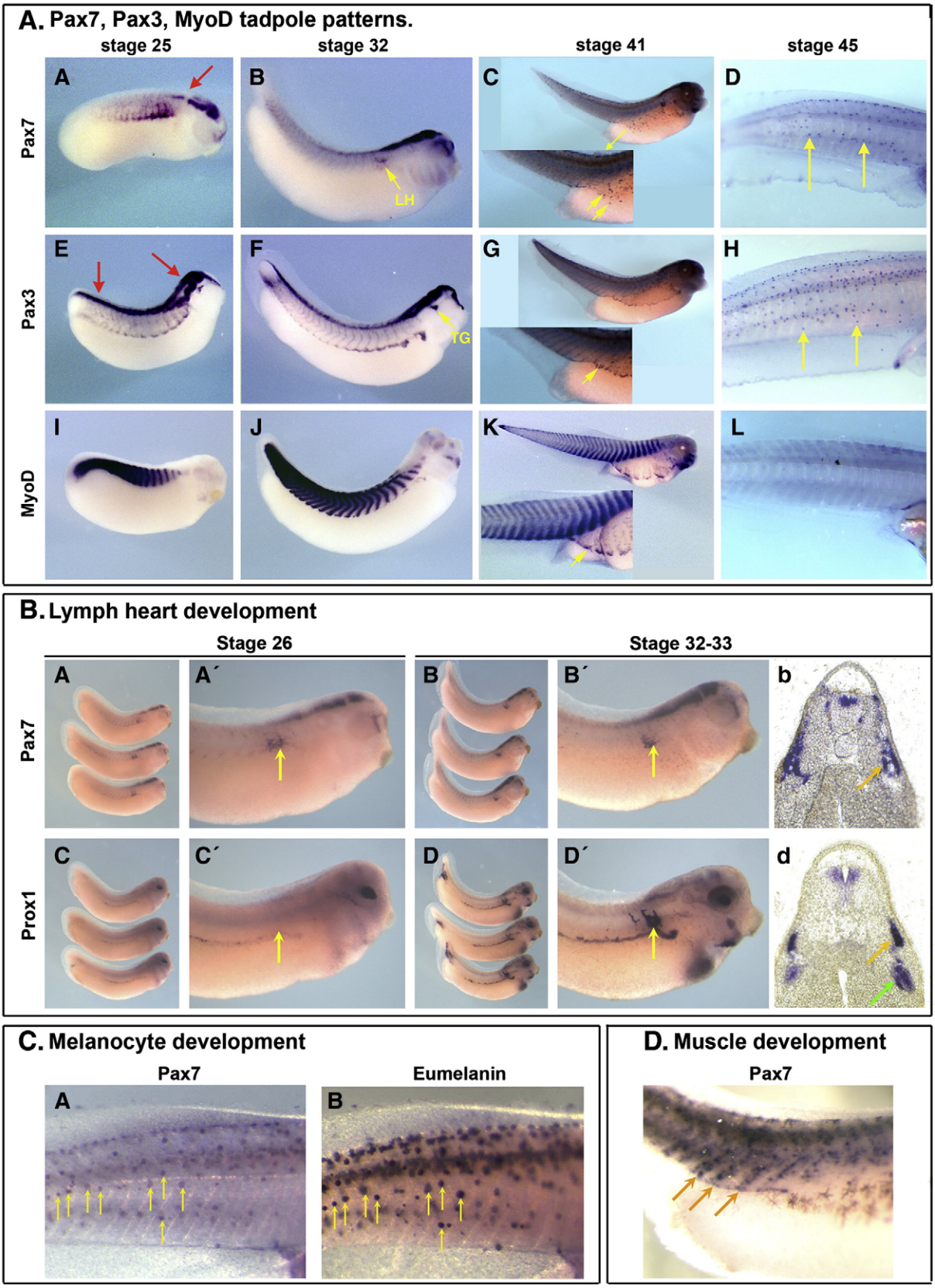

rescue was observed. Embryos injected with Pax7MO lost *snail2* expression (95% strong decrease, $n=20$, Fig. 7L). In contrast, co-injections resulted in restored *snail2* expression (50% normal, 50% mild decrease, $n=18$, Fig. 7M).

Thus, we show here that Pax7 function is essential for full neural crest formation. However, as we did not observe *pax7* expression at the neural border or in the neural crest progenitors themselves, we have proposed two hypotheses in order to explain how Pax7 may control neural crest formation: Pax7 may be important for central nervous system patterning along the anterior–posterior axis, and thus secondarily influence neural crest formation at the edge of the posterior domain; alternatively, Pax7 may be important for paraxial mesoderm development and thus secondarily in its inductive function in neural crest early development. We have explored these two hypotheses below.

Pax7 controls brain patterning by maintaining midbrain and hindbrain fates

In order to analyze brain patterning, we have looked at four regional markers: *otx2* which labels the forebrain and midbrain (Fig. 8A); *gbx2* and *engrailed2 (en2)* which mark the mid–hindbrain boundary (Figs. 8F, K); and *krox20* for the hindbrain (Fig. 7). At early neurula stage (stages 12–13), *otx2* and *gbx2* expression were normal after Pax7 unilateral depletion (not shown), suggesting that the initial onset of neural anterior–posterior patterning occurs normally (Tour et al., 2002a), and in agreement with the late onset of *pax7* expression (Fig. 1). At mid-late neurula stages, unilateral Pax7MO injections resulted in *otx2* expansion in more posterior areas (69.2%, $n=65$; Figs. 8B–D), while *gbx2*, *en2* and *krox20* were either shifted posteriorly or lost (respectively 89.3%, $n=28$ for *gbx2*, 69%, $n=52$ for *en2* and 95%, $n=61$ for *krox20*; Figs. 7B, C and 8G–I, L–N). Pax7EnR mRNA injections resulted in a similar phenotype: *otx2* expansion in 84.6% of the embryos ($n=104$; Fig. 8D) and diminished *en2* (69%, $n=52$; Fig. 8N) and *krox20* (70%, $n=57$; Fig. 7D). In this case, *gbx2* expression was only slightly shifted posteriorly (Fig. 8I). In contrast to Pax7 depletion phenotype, Pax3MO did not perturb *otx2* pattern (symmetrical expression in 72% of the injected embryos, $n=50$). However, Pax3 depletion had similar posterior shifting or loss on *gbx2* (75%, $n=28$; Fig. 8J), *en2* (73%, $n=11$; Fig. 8O) and *krox20* (75%, $n=45$; Fig. 7E). In conclusion, these experiments uncover a novel role for Pax7 in maintaining the mid–hindbrain boundary (prospective isthmus) and hindbrain fates and preventing the posterior expansion of forebrain and midbrain fates during early brain patterning (at stage of neural closure). In relationship to neural crest patterning, this altered midbrain and hindbrain patterning could secondarily result into defective neural crest induction.

Pax7 is needed for neural crest induction by the paraxial mesoderm

Morphological and *myoD* analysis of Pax7 morphants suggests that Pax7 loss has profound effects on paraxial mesoderm development (Fig. 6). Paraxial mesoderm signaling activity is essential during neural crest induction (Bonstein et al., 1998; Monsoro-Burq et al., 2003). Defective paraxial mesoderm, after Pax7 depletion, could impair neural crest induction in the overlying ectoderm, and thus suggest how Pax7 depletion may affect neural crest induction. To address this issue, we have used heterochronic recombinants, using ectoderm from the blastocoel roof from a stage 9 blastula embryo, recombined with the dorsal–lateral marginal zone (prospective paraxial mesoderm) of a stage 10.25 early gastrula. This assay results in potent *snail2* and other neural crest marker induction in the ectoderm, as well as melanocyte differentiation later on (Bonstein et al., 1998; Monsoro-Burq et al., 2003) (Figs. 9A, D; G, lane5). Ectoderm (Figs. 9B; G, lane 3) or paraxial mesoderm (Figs. 9C; G, lane 4) explants grown in isolation, do not express *snail2*. When the ectoderm was dissected from Pax3MO injected embryos, *snail2* induction was strongly impaired (Fig. 9G, lane 6) while Pax7MO in the ectoderm did not prevent *snail2* induction (Fig. 9G, lane 7). In sharp contrast, depletion of Pax3 in the paraxial mesoderm did not alter *snail2* induction, despite defective *muscle actin* specification (Figs. 9F, G, lane 8). Moreover, Pax7 function in the paraxial mesoderm explant is essential for *snail2* induction in the ectoderm, as well as for proper *muscle actin* expression (Figs. 9E; G, lane 9; F).

The results above suggested that Pax3 and Pax7 act in different tissues during neural crest induction. This does not rule out that the two proteins could have similar functions. To address if they display redundant functions, we have attempted to rescue Pax3 and Pax7 knock-down by Pax7 and Pax3 gain of function respectively. In both situations, while the homologous gain of function (Pax3 for Pax3MO and Pax7 for Pax7MO) restored *snail2* expression, neither Pax3 nor Pax7 were able to compensate for the knock-down of Pax7 or Pax3 respectively (Fig. 10). This was also true when a later stage was considered: Pax7 did not rescue the loss of melanocytes observed in the Pax3 morphants. All these data suggest that Pax3 and Pax7 exert distinct functions, in distinct tissues in early and later neural crest development in *Xenopus*.

Finally, as we observed that *myod* expression was defective in Pax7 morphants (Fig. 6), we asked if the effect of Pax7 in the paraxial mesoderm was due to altered mesoderm patterning. We examined the paraxial mesoderm markers *myoD* and *muscle actin* and the ventral mesoderm marker *vent1* in the recombinants (Fig. 9G). We found that both in Pax3 and Pax7-depleted dorsal–lateral marginal zone mesoderm, paraxial patterning is defective and that ventral marker *vent1* is higher than in controls at neurula stage. However, we did not find a molecular difference between Pax3 and Pax7 morphant mesoderm that could account for their distinct neural crest inducing ability.

In conclusion, these results show a dramatic difference in the mode of activity of Pax7 and Pax3 in neural crest induction, Pax7 being essential for the inductive signaling from the paraxial mesoderm, while Pax3 is needed in the ectoderm.

Discussion

In this work, we address *pax7* pattern regulation in the brain of *X. laevis* embryos, and Pax7 function in neural and neural crest early development. We provide a parallel analysis of Pax3 and Pax7 function, using a specific antisense morpholino strategy, which uncovers both common and distinct functions for these two paralogous genes. In particular, both genes are important for neural crest induction, but they act by two strikingly different mechanisms.

Pax7 is expressed in a spatially restricted pattern in X. laevis central nervous system, and is activated by posteriorizing signals and Pax3

Pax3 and Pax7 have diverged early in vertebrate evolution; their sequences can be clearly grouped on a phylogenetic tree, and specific primers, probes and morpholinos can be designed (Fig. 1, Supplemental

Fig. 5. *Pax7* expression in tadpoles. A/ At tailbud stage (st. 25–32) *pax7* exhibits a dynamic expression in the myotome, which vanishes at late stage, while brain and spinal cord expression remains restricted to hindbrain and anterior spinal cord (A–B). *Pax7* is also found in the lymph heart (B, arrow). This contrasts to *pax3* expression in the entire length of the spinal cord, in the hypaxial muscle and trigeminal ganglia (E–F, arrows) or to *myod* expression in the epaxial muscles (I–J). At swimming tadpole stage (st 41–45), *pax7* is expressed in scattered cells on the side of the embryo (yellow arrows) and cells that align at the edge of the myotome cells (see D/), while *pax3* and *myod* mark muscle (G, K). Both *pax7* and *pax3*, but not *myod*, label melanocytes (D, H, L). B/ During lymph heart development, *pax7* is detected earlier than the lymph heart marker *prox1* (A, A′, C, C′). By stage 33, both *pax7* and *prox1* expression overlap in the lymph heart (B, B′, D, D′ and transverse sections b, d, yellow arrows), while *prox1* is also expressed adjacent to the cardinal vein (green arrow; Ny et al., 2005). C/ Late tadpoles where photographed before bleaching to position the melanocytes (B) and then *pax7* was revealed (A). Most melanocytes were labelled by *pax7* (yellow arrows). D/ Some *pax7*-positive cells aligned at the edge of each myotome in stage 41 tadpoles and may constitute the prospective satellite cell population (arrows).

Figs. 1 and 2). Their respective expression in the alar plates of the central nervous system, in the migrating neural crest and in the paraxial mesoderm varies according to the different species described, suggesting that the respective functions within the Pax3/7 subfamily could vary in different species. We provide here the first precise comparison of Pax3 and Pax7 expression in *X. laevis*.

In *X. laevis*, *pax7* and *pax3* display clearly distinct expression patterns and *pax7* pattern differs in several respects from *pax7*

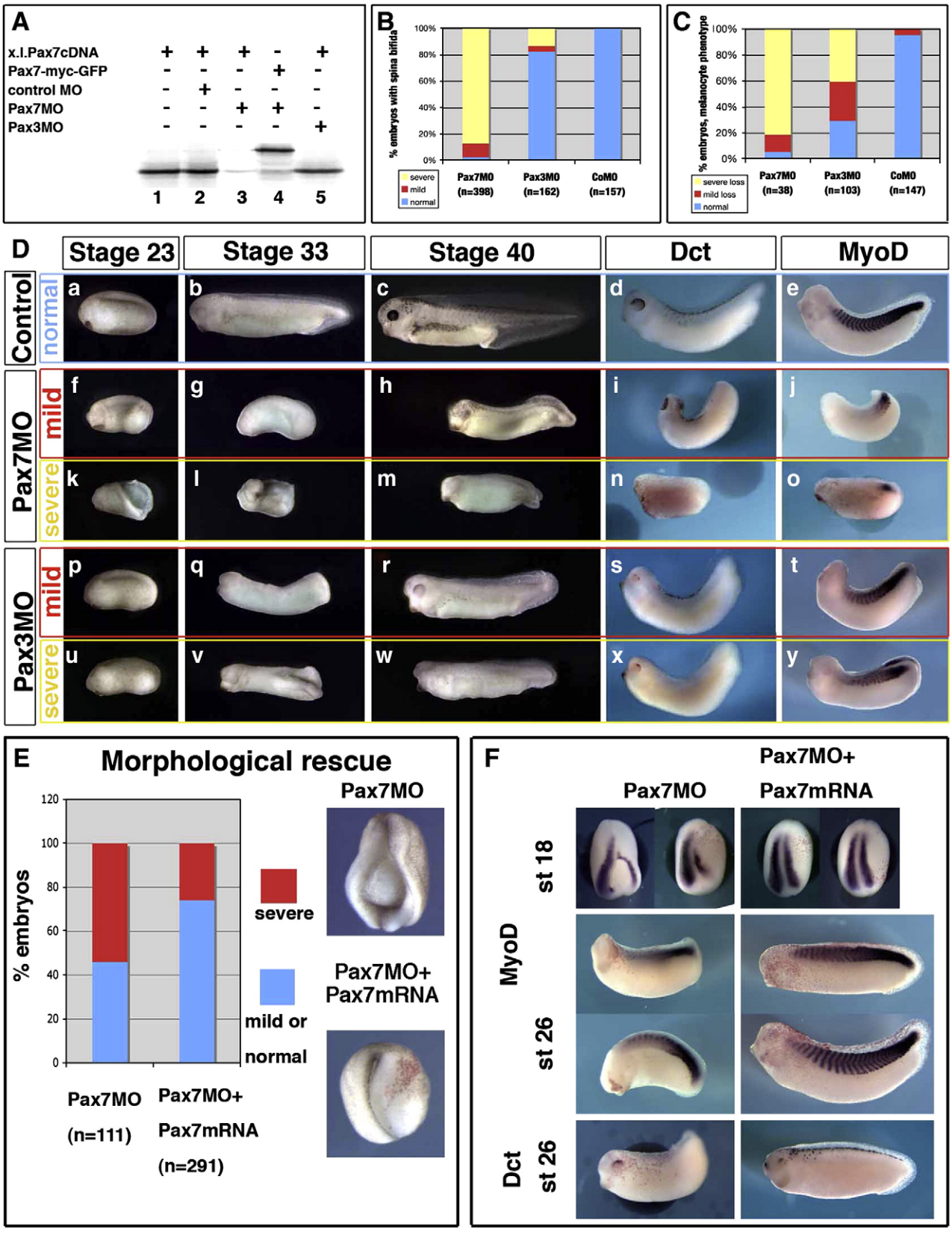

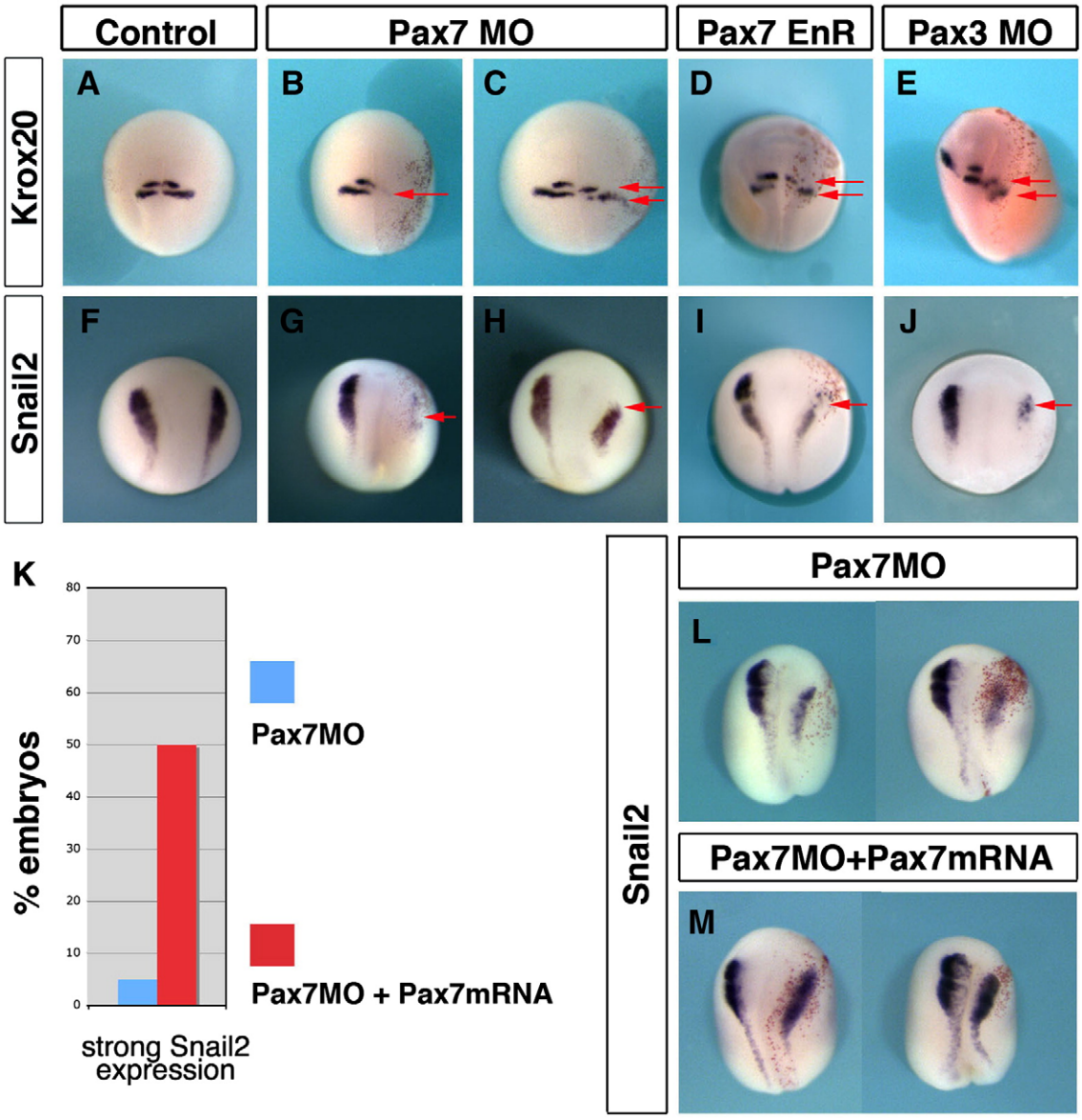

Fig. 7. Pax7 and Pax3 are essential for hindbrain and neural crest patterning. The early phenotype of Pax7 morphants was analyzed at stage 18. Control siblings show normal expression of *krox20* (A) and *snail2* (F). Pax7 morphants exhibit either a severe loss of *krox20* (B) and *snail2* (G), or a posterior shift of rhombomeres r3 and r5 (C, arrows) accompanied by reduced *snail2* expression (H). A similar phenotype is observed in Pax7EnR injected embryos (D, I) or Pax3 morphants (E, J). Pax7MO phenotype is rescued by injection of Pax7-myc mRNA), insensitive to the morpholino (Fig. 6): *snail2* expression is restored (L shows two morphants and (M) two siblings injected with MO and the rescue construct).

expression in other vertebrates. During early-mid-neurulation, only *pax3* is detected, either by RT-PCR using specific primers, or by in situ hybridization (Fig. 1). *Pax3* is present in the prospective hatching gland, the lateral aspect (alar plates) of the neural plate comprising the prospective neural crest domain. In contrast, the *pax7* expression appears in the paraxial mesoderm and in the midbrain and hindbrain at later neurulation stages, which differs from observations of Pax7 expression in the chick gastrula stages (Basch et al., 2006). *Pax7* is neither detected in the prospective neural crest domain nor in the migrating neural crest. This later onset of *pax7*, after neural tube closure, is also observed in lamprey, zebrafish, chick and mouse neurulae (Mansouri et al., 1996; Matsunaga et al., 2001; McCauley and Bronner-Fraser, 2002; Minchin and Hughes, 2008). However, *pax7* expression in a small subpopulation of migrating cranial neural crest cells is seen in zebrafish, chick and mouse embryos (Mansouri et al., 1996; Matsunaga et al., 2001; Minchin and Hughes, 2008).

These two initial expression patterns in the CNS resolve into two distinct domains, *pax3* being detected along the entire anterior–

Fig. 6. Pax7 morphants are affected in earlier stages than Pax3 morphants, although both display mesoderm and neural crest defects. (A) Pax7MO blocks in vitro translation of *pax7* (lane 3) but neither that of a *pax7-gfp* fusion lacking the MO-binding sequence (lane 4), nor of *pax3* (5). (B) Pax7 morphants display early and severe elongation defects shortly after gastrulation (yellow), while a few of them exhibit milder phenotypes allowing us to follow their development further (red). In contrast, Pax3 morphants are rather normal until the end of neurulation except for posterior spina bifida in the more severely affected ones (yellow). (C) Melanocyte development was analyzed in later stage embryos, among the mild phenotype for Pax7 morphants, and in Pax3 morphants. Severe loss refers to the lack of *dct* positive or pigmented cells, while "mild loss" refers to decreased melanocyte number associated to lack of melanocyte migration. (D) Sibling control embryos (a–e), Pax7 morphants with mild (f–j) or severe (k–o) phenotype, Pax3 morphants with mild (p–t) or severe (u–y) phenotype were analyzed at the end of neurulation (stage 23), tailbud stage 33 or swimming tadpole stage 45, and stained for *dct* and *myod* at stage 33. They display prominent head, brain, mesoderm and melanocytes defects. (E)The Pax7MO phenotype is rescued by co-injections with Pax7-myc mRNA, insensitive to the morpholino. See text for details. (F) Both *myoD* and *dct* expression are rescued by *pax7* mRNA injection into Pax7 morphants (see text for details).

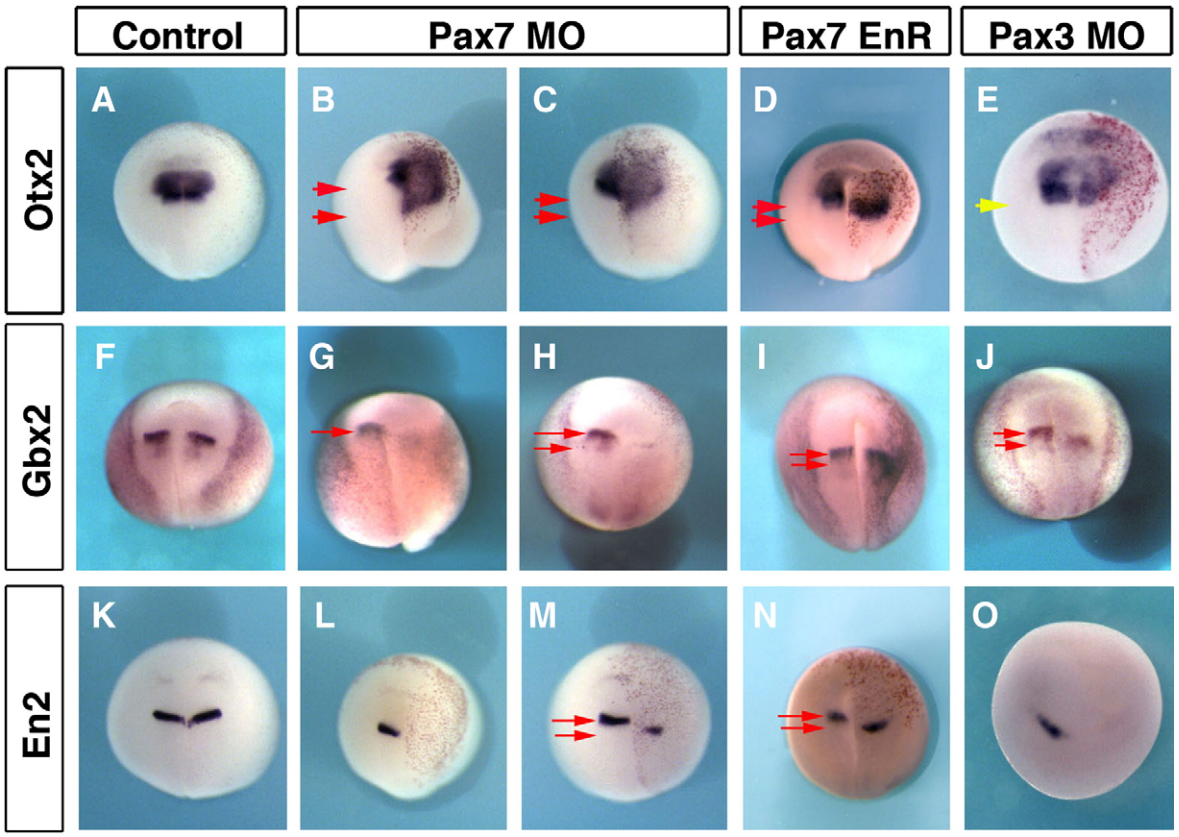

Fig. 8. Pax7 and Pax3 regulate mid–hindbrain boundary maintenance. Pax7 depletion leads to forebrain–midbrain expansion as seen by *otx2* posterior expansion (B, C). This is accompanied by loss or posterior shift of the mid–hindbrain boundary (*Gbx2*, G, H) and *En2* (L, M). A similar phenotype is observed after PaxEnR (D, I, N). Pax3 morphants do not exhibit expanded *otx2* domain (E, yellow arrow indicates similar posterior boundaries on each side), but they also display defective or shifted mid–hindbrain boundary (J, O). Red arrows indicate the extent of shift between the posterior boundary on control non-injected (left) side, and the shifted boundary on injected (right) side.

posterior axis, while *pax7* is expressed locally in the midbrain, hindbrain and anteriormost spinal cord, but not in rest of the spinal cord (Fig. 2). This strikingly differs from expression of both Pax3 and Pax7 all along the neuraxis in chick and mouse, but is similar to the described pattern in shark, zebrafish, and salmon (Borycki et al., 1999; Freitas et al., 2006; Goulding et al., 1993a; Minchin and Hughes, 2008; O'Neill et al., 2007; Sibthorpe et al., 2006). Additional differences include that *pax7* does not label the trigeminal ganglia as *pax3* does (Baker et al., 2002) and *pax7* – but not *pax3* – is expressed in the lymph heart (Ny et al., 2005) (Fig. 5). Both *pax3* and *pax7* are expressed in melanocytes in *Xenopus* (Fig. 5) whereas they differentially label both melanophores and xanthophores in zebrafish (Minchin and Hughes, 2008).

In contrast, the expression of *pax3* and *pax7* in the paraxial mesoderm, respectively in the hypaxial and the superficial myotome (Figs. 2 and 5), is in agreement with expression in other vertebrates (Borycki et al., 1999; Goulding et al., 1993b). In mouse embryos, distinct enhancers control the distinct regions of *pax7* expression in brain and neural crest derivatives (Lang et al., 2003). Our expression pattern analysis in *Xenopus* suggests that evolution has acted differentially on these enhancers.

We have explored the possibility that the differences in *pax7* expression compared to other species, in particular in the spinal cord, could be due to different response to the posteriorizing signals that pattern the neural plate, namely FGF, Wnt and retinoid signaling. We have found that *pax7* expression is modulated by these three pathways, similarly to other genes expressed in the posterior neural cells, such as *pax3*, *hoxb9* or *snail2* (Fig. 3 and data not shown). The restricted pattern observed for *pax7* could nonetheless depend on lower sensitivity to endogenous signaling levels rather than qualitatively different response. Additionally, we did not observe a significant role of FGF signaling at the time of isthmus formation (Supplemental Fig. 3), suggesting that general early anterior–posterior patterning broadly controls *pax7* among other neural restricted markers.

In Splotch mutant mice, *pax7* expression in the somites and spinal cord is upregulated (Borycki et al., 1999). Here we show that Pax3, which expression domain comprises that of *pax7*, positively controls *pax7* expression in the brain, in parallel to general development of the alar plates (Fig. 4). We did not observe broad ectopic expression in the spinal cord after Pax3 misexpression (Fig. 4), suggesting that regulation by Pax3 is active only in the brain and anterior spinal cord, i.e. around *pax7* normal domain, compared to the mouse situation.

Although not expressed in neural crest progenitors, Pax7 is essential for brain, neural crest and myotome patterning

Pax3 and Pax7 play an essential role in neural crest induction in *Xenopus* and chick embryos respectively (Basch et al., 2006; Monsoro-Burq et al., 2005; Sato et al., 2005). Moreover, Pax7 and Pax3 are thought to display redundant activities in the mouse neural crest, since the replacement of *pax7* in the *pax3* locus suffices to rescue the neural/neural crest phenotype, while the paraxial mesoderm phenotype remains severe (Relaix et al., 2004). Here, we have explored the possibility that Pax7 displays a similar function to Pax3 in *Xenopus* neurulae. Surprisingly, *pax7* was not detected in the neural fold at the time of neural crest induction (late gastrula, early neurula) when *pax3* is abundantly expressed (Fig. 1). At later stages, neither *pax3* nor *pax7* transcripts are detected in the migrating neural crest (Fig. 2). This expression contrasts with the pattern in chick and mouse embryos (Basch et al., 2006; Mansouri et al., 1996). Later on, however, both *pax3*

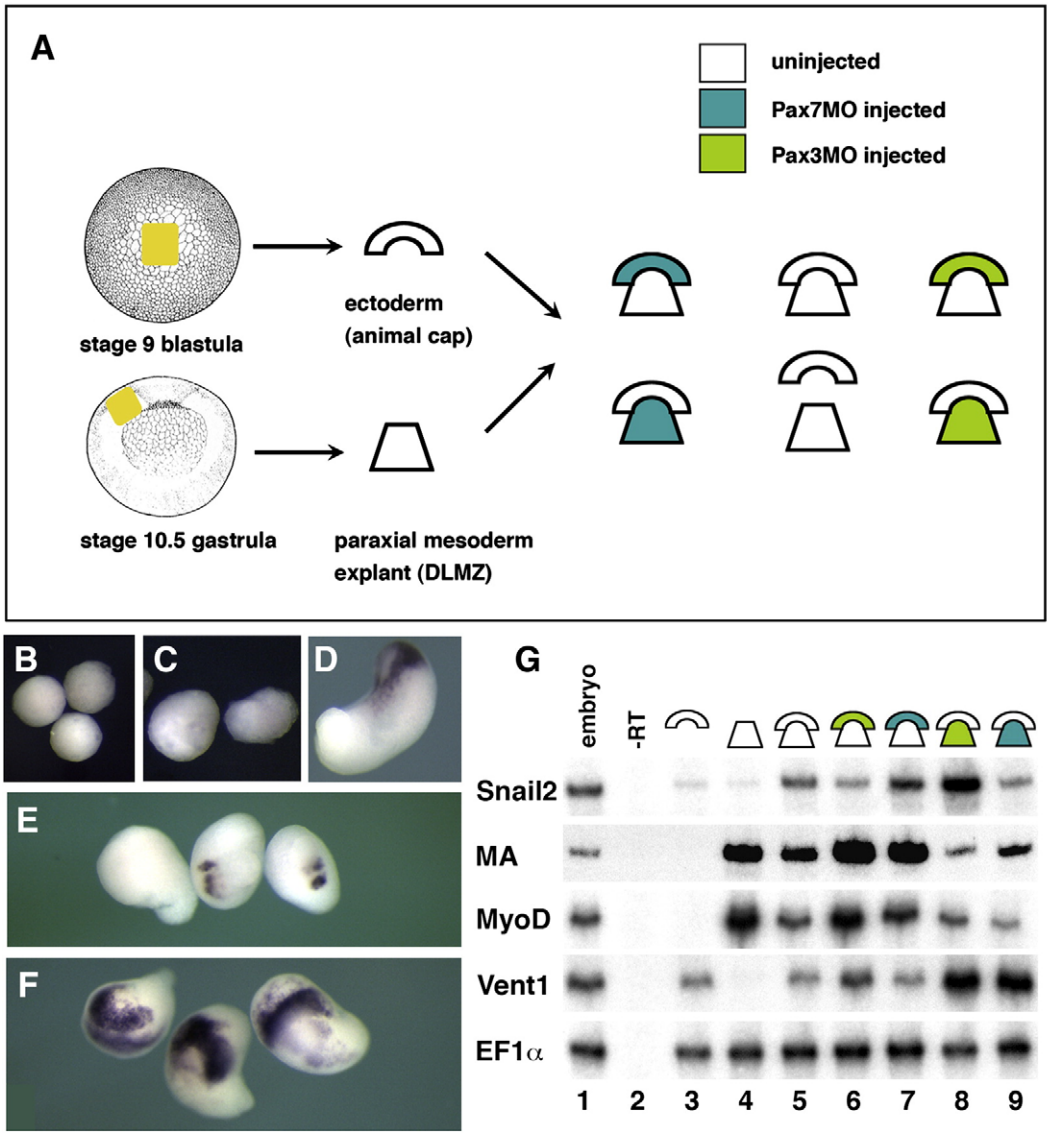

Fig. 9. Pax7 is essential for the neural crest inducing activity of the paraxial mesoderm, while Pax3 acts in the ectoderm. (A) We have recombined the stage 9 blastocoel roof ectoderm to stage 10.25 prospective paraxial mesoderm (dorsal–lateral marginal zone), a classical assay for neural crest induction in the ectoderm. Ectoderm and DLMZ were dissected from either control uninjected or Pax3 or Pax7 morphants (see color code). Ectoderm (B) or DLMZ (C) grown alone until stage 18 do not express *snail2*, while the recombined explants (D) do. When the DLMZ comes from Pax7 morphant (E), *snail2* induction is strongly impeded, while Pax3 depleted DLMZ do not perturb *snail2* induction (F). RT-PCR analysis (G) further shows that ectoderm alone (lane 3) does not express *snail2*, *myoD* or *muscle actin* (MA), DLMZ alone expresses only *myoD* and *MA* (lane 4) while the recombinant expresses both (lane 5). *Snail2* induction is impaired if the ectoderm is depleted for Pax3 (lane 6) but not for Pax7 (lane 7). In contrast, *snail2* induction is normal if DLMZ comes from Pax3 morphants (lane 8) but is impaired for Pax7 depleted DLMZ (lane 9). In both Pax3- and Pax7-depleted DLMZ, *myoD* and *MA* expression are decreased while *vent1* is abnormally upregulated.

and *pax7* are expressed in the melanocytes (Fig. 5) as described in several other species (Lacosta et al., 2005; Minchin and Hughes, 2008).

However, rather surprisingly, although we did not find *pax7* expression in the neural crest progenitors, our knock-down experiments show that Pax7 depletion dramatically affects embryo elongation, brain, and neural crest development. *Dct* and *myoD* expression analysis confirmed that myotome and pigment formation were severely affected, the Pax7 phenotypes being even more dramatic than that of Pax3 depletion, and rescued by adding back Pax7 transcripts (Fig. 6). Additionally, neural crest and brain induction and early patterning are strongly affected (Figs. 7 and 8). This is in contrast to the Pax7 mouse mutants, or with zebrafish morphants, which only display a mild and late phenotype (Mansouri et al., 1996; Minchin and Hughes, 2008). In mouse, *pax3* and *pax7* patterns overlap largely and Pax3 and Pax7 exert redundant functions; in zebrafish, *pax7* has a late onset after initial neural and mesoderm patterning. We have tested possible functional redundancy between Pax3 and Pax7 in *Xenopus*, by attempting to rescue Pax3 and Pax7 knock-downs by Pax7 and Pax3 respectively (Fig. 10): Pax3 did not rescue *snail2* expression in Pax7 morphants, nor did Pax7 rescue *snail2* expression or melanocyte differentiation in Pax3 morphants. Our results, compared to those in the other species, strongly suggest a re-distribution of functions between Pax3 and Pax7 in vertebrates. Such gene function re-shuffling as has also been described for Snail family members (Sefton et al., 1998).

Pax7 participates in neural crest induction via its role in brain and paraxial mesoderm patterning

We have analyzed Pax3 and Pax7 respective roles in early brain patterning, at times of isthmus formation. We show that both genes are essential activators to allow the maintenance of the mid–

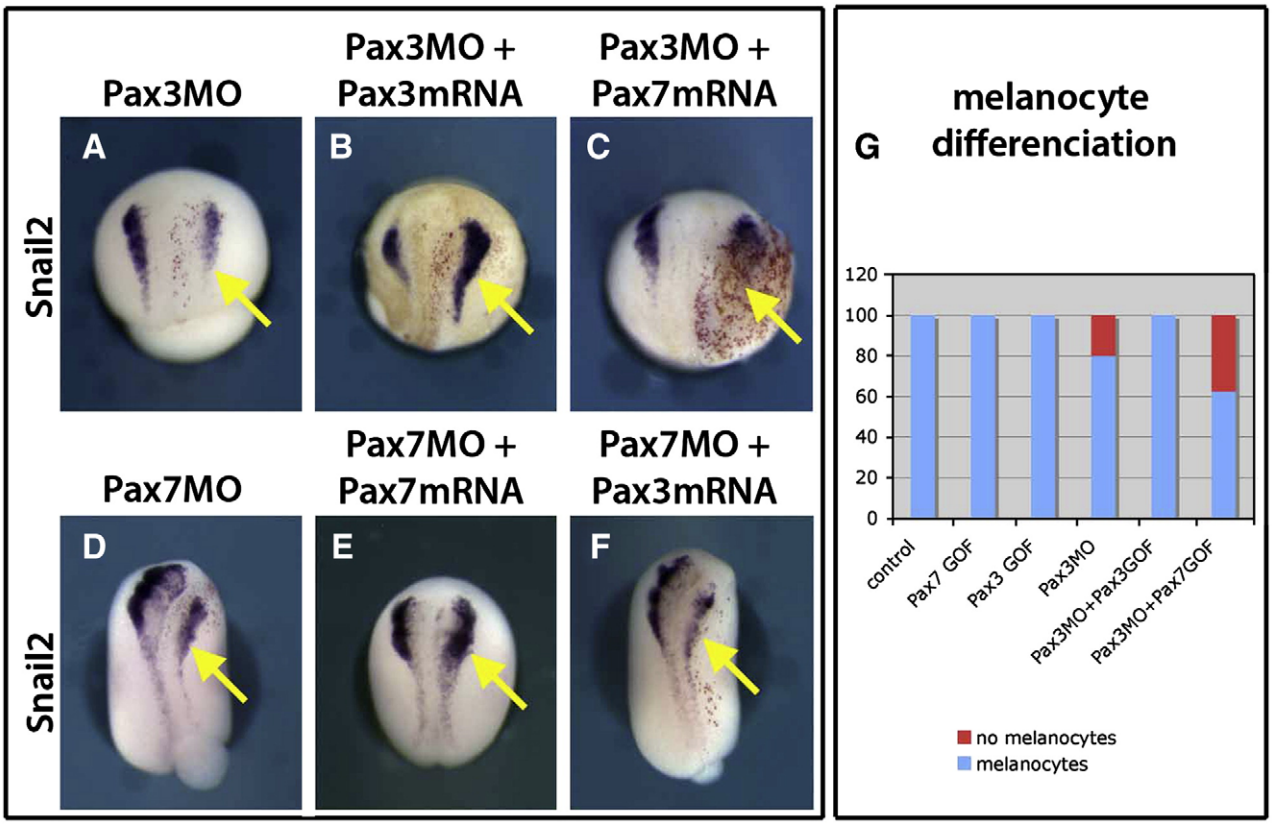

Fig. 10. Pax3 and Pax7 do not display redundant functions in neural crest induction and development. Pax3 morphant phenotype (A) is rescued by gain of function for Pax3 (B) but not Pax7 (C). At a later stage, Pax7 does not restore melanocyte development in Pax3 morphants either (G). Conversely, Pax3 is not sufficient to rescue Pax7 depletion (D, F), in contrast to Pax7 gain of function (E). These data indicate that the two proteins do not display similar roles in neural crest induction and development. Injected side is on the right (yellow arrow).

hindbrain boundary (Gbx2, En2) and hindbrain (Krox20) patterning, and that Pax7 specifically prevents ectopic posterior expansion of *otx2*. Otx2 specifies forebrain–midbrain fates (Rhinn et al., 1999; Tour et al., 2002b). *Otx2* and *gbx2* domains are initially set up shortly after the start of neurulation and the two factors exert reciprocal negative regulation that defines the border between their respective domains, this border being the mid–hindbrain boundary (Acampora et al., 2001; Tour et al., 2002a; Ye et al., 2001). The onset of *otx2* and *gbx2* domains is initiated normally in presence of Pax7MO (stages 12–14), but the maintenance of this boundary is perturbed (*en2*) as well as hindbrain patterning (*krox20*) and cranial neural crest formation (*krox20*, *snail2*) (Figs. 7 and 8). Pax3 depletion has a similar outcome on hindbrain formation, although Pax3 does not seem to restrict *otx2* expression (Fig. 8), in agreement with *pax3* expression pattern in the forebrain (Figs. 1 and 2). Our results from depletion analysis correlate with the phenotypes obtained by gain of function in chicken embryos: Pax3/7 electroporation promotes ectopic anterior hindbrain and optic tectum development in the diencephalon (Matsunaga et al., 2001). Hence we show here that Pax3 and Pax7 cooperate to promote early hindbrain development, a major source of cranial neural crest progenitors (Creuzet et al., 2005).

In addition to interactions within the ectoderm–neurectoderm layer, neural crest induction requires signals from paraxial mesoderm (Bonstein et al., 1998; Monsoro-Burq et al., 2003). We observe here severe defects in mesoderm formation and axis elongation in the Pax7 morphants, suggesting that the neural crest inducing function of paraxial mesoderm might be altered as well (Fig. 6). By using an explant recombination strategy, we show that Pax3 and Pax7 participate in neural crest induction by two distinct mechanisms: Pax3 activity is essential in the ectoderm, confirming previous work on Pax3 role in *Xenopus* neural crest induction (Monsoro-Burq et al., 2005; Sato et al., 2005); while Pax7 acts in the paraxial mesoderm, which in turn promotes induction in the ectoderm (Fig. 9). Given the relatively late onset of Pax7 expression, compared to neural crest induction, our data also suggest that Pax7-mediated paraxial mesoderm induction participates in maintaining or amplifying the initial Pax3-mediated neural crest induction in the ectoderm. Thus, the two genes cooperate in neural crest induction, but by two distinct strategies (Figs. 9 and 10). In addition, the roles of Pax3 and Pax7 in the ectoderm have been exchanged between species, when *Xenopus* and chick are compared (Basch et al., 2006). Our observations also show that Pax3 and Pax7 do not play redundant roles in the paraxial mesoderm (Fig. 6 and Supplemental Fig. 3), similar to the mouse situation (Relaix et al., 2004), but here, their relative importance in the mesoderm seems to be swapped since the Pax7 depletion has earlier and more profound effects than Pax3 loss, which is opposite to the mouse mutant (Mansouri et al., 1996; Relaix et al., 2004).

In conclusion, our study analyzes how the functions of two closely related Pax3 and Pax7 paralogs have been distributed in the amphibian *X. laevis*, during neural and neural crest induction. We use their strikingly distinct expression patterns, in the brain, the spinal cord and in the paraxial mesoderm of *Xenopus* embryos to experimentally explore their specific function in each of these tissues, in the absence of redundant activity of the other paralog. We show that Pax3 and Pax7 cooperate in mid–hindbrain boundary formation, by promoting hindbrain fates, and that Pax7 specifically restricts *otx2* expression. Additionally, Pax3 and Pax7 cooperate to trigger neural crest induction, by acting in the ectoderm and in the mesoderm respectively.

Acknowledgments

The authors are grateful to Dr Clare Baker for her critical reading of the manuscript, to Dr J. Slack for his generous gift of Pax7-EnR clone, and to the Monsoro-Burq laboratory members for their comments and support. This work was initiated in RMH's laboratory with funding from NIH GM42341. This work was funded by grants from the CNRS (ATIP Program), Ligue contre le Cancer, Association pour la Recherche contre le Cancer (ARC), and Fondation de France to A.H. M.-B. S. M. was funded by the Institut Curie. D. R. was funded by Fondation de France, Region Ile de France and Institut Curie.

Appendix A. Supplementary data

Supplementary data associated with this article can be found, in the online version, at doi:10.1016/j.ydbio.2010.01.022.

References

Acampora, D., Gulisano, M., Broccoli, V., Simeone, A., 2001. Otx genes in brain morphogenesis. Prog. Neurobiol. 64, 69–95.
Auerbach, R., 1954. Analysis of the developmental effects of a lethal mutation in the house mouse. J. Exp. Zool. 127, 305–329.
Baker, C.V., Stark, M.R., Bronner-Fraser, M., 2002. Pax3-expressing trigeminal placode cells can crest sites but are committed to a cutaneous sensory. Dev. Biol. 249, 219–236.
Basch, M.L., Bronner-Fraser, M., Garcia-Castro, M.I., 2006. Specification of the neural crest occurs during gastrulation and requires Pax7. Nature 441, 218–222.
Blumberg, B., Bolado Jr., J., Moreno, T.A., Kintner, C., Evans, R.M., Papalopulu, N., 1997. An essential role for retinoid signaling in anteroposterior neural patterning. Development 124, 373–379.
Bonstein, L., Elias, S., Frank, D., 1998. Paraxial-fated mesoderm is required for neural crest induction in *Xenopus* embryos. Dev. Biol. 193, 156–168.
Borycki, A.G., Li, J., Jin, F., Emerson, C.P., Epstein, J.A., 1999. Pax3 functions in cell survival and in pax7 regulation. Development 126, 1665–1674.
Bradley, L.C., Snape, A., Bhatt, S., Wilkinson, D.G., 1993. The structure and expression of the *Xenopus* Krox-20 gene: conserved and divergent patterns of expression in rhombomeres and neural crest. Mech. Dev. 40, 73–84.
Buckingham, M., 2006. Myogenic progenitor cells and skeletal myogenesis in vertebrates. Curr. Opin. Genet. Dev. 16, 525–532.
Chalepakis, G., Goulding, M., Read, A., Strachan, T., Gruss, P., 1994a. Molecular basis of splotch and Waardenburg Pax-3. Proc. Natl. Acad. Sci. USA 91, 3685–3689.
Chalepakis, G., Jones, F.S., Edelman, G.M., Gruss, P., 1994b. Pax-3 contains domains for transcription activation and transcription inhibition. Proc. Natl. Acad. Sci. USA 91, 12745–12749.
Chang, C., Hemmati-Brivanlou, A., 1998. Neural crest induction by Xwnt7B in *Xenopus*. Dev. Biol. 194, 129–134.
Chen, Y., Lin, G., Slack, J.M., 2006. Control of muscle regeneration in the *Xenopus* tadpole tail by Pax7. Development 133, 2303–2313.
Creuzet, S., Couly, G., Le Douarin, N.M., 2005. Patterning the neural crest derivatives during development of the vertebrate head: insights from avian studies. J. Anat. 207, 447–459.
Delaune, E., Lemaire, P., Kodjabachian, L., 2005. Neural induction in *Xenopus* requires early FGF signalling in addition to BMP inhibition. Development 132, 299–310.
Epstein, D.J., Vekemans, M., Gros, P., 1991. Splotch (Sp2H), a mutation affecting development of the mouse neural tube, shows a deletion within the paired homeodomain of Pax-3. Cell 67, 767–774.
Fletcher, R.B., Harland, R.M., 2008. The role of FGF signaling in the establishment and maintenance of mesodermal gene expression in *Xenopus*. Dev. Dyn. 237, 1243–1254.
Fletcher, R.B., Baker, J.C., Harland, R.M., 2006. FGF8 spliceforms mediate early mesoderm and posterior neural tissue formation in *Xenopus*. Development 133, 1703–1714.
Franz, T., Kothary, R., 1993. Characterization of the neural crest defect in Splotch (Sp1H) mutant mice using a lacZ transgene. Brain Res. Dev. Brain Res. 72, 99–105.
Freitas, R., Zhang, G., Cohn, M.J., 2006. Evidence that mechanisms of fin development evolved in the midline of early vertebrates. Nature 442, 1033–1037.
Goulding, M.D., Chalepakis, G., Deutsch, U., Erselius, J.R., Gruss, P., 1991. Pax-3, a novel murine DNA binding protein expressed neurogenesis. EMBO J. 10, 1135–1147.
Goulding, M.D., Lumsden, A., Gruss, P., 1993a. Signals from the notochord and floor plate regulate expression of two Pax genes in the developing spinal. Development 117, 1001–1016.
Goulding, M.D., Lumsden, A., Gruss, P., 1993b. Signals from the notochord and floor plate regulate the region-specific expression of two Pax genes in the developing spinal cord. Development 117, 1001–1016.
Goulding, M., Lumsden, A., Paquette, A.J., 1994a. Regulation of Pax-3 expression in the dermomyotome and its role in muscle development. Development 120, 957–971.
Goulding, M., Lumsden, A., Paquette, A.J., 1994b. Regulation of Pax-3 expression in the dermomyotome development. Development 120, 957–971.
Grammer, T.C., Liu, K.J., Mariani, F.V., Harland, R.M., 2000. Use of large-scale expression cloning screens in the *Xenopus laevis* tadpole to identify gene function. Dev. Biol. 228, 197–210.
Gruss, P., Walther, C., 1992. Pax in development. Cell 69, 719–722.
Hemmati-Brivanlou, A., de la Torre, J.R., Holt, C., Harland, R.M., 1991. Cephalic expression and molecular characterization of *Xenopus* En-2. Development 111, 715–724.
Holland, L.Z., Schubert, M., Kozmik, Z., Holland, N.D., 1999. AmphiPax3/7, an amphioxus paired box gene: insights into chordate myogenesis, neurogenesis, and the possible evolutionary precursor of definitive vertebrate neural crest. Evol. Dev. 1, 153–165.
Hopwood, N.D., Pluck, A., Gurdon, J.B., 1989. MyoD expression in the forming somites is an early response to mesoderm induction in *Xenopus* embryos. EMBO J. 8, 3409–3417.
Jostes, B., Walther, C., Gruss, P., 1990. The murine paired box gene, Pax7, is expressed specifically during the development of the nervous and muscular system. Mech. Dev. 33, 27–37.
Kintner, C.R., Brockes, J.P., 1984. Monoclonal antibodies identify blastemal cells derived from dedifferentiating limb regeneration. Nature 308, 67–69.
Koebernick, K., Kashef, J., Pieler, T., Wedlich, D., 2006. *Xenopus* Teashirt1 regulates posterior identity in brain and cranial neural crest. Dev. Biol. 298, 312–326.
Krieg, P.A., Varnum, S.M., Wormington, W.M., Melton, D.A., 1989. The mRNA encoding elongation factor 1-alpha (EF-1 alpha) is a major transcript at the midblastula transition in *Xenopus*. Dev. Biol. 133, 93–100.
Kuang, S., Rudnicki, M.A., 2008. The emerging biology of satellite cells and their therapeutic potential. Trends Mol. Med. 14, 82–91.
Kumasaka, M., Sato, S., Yajima, I., Yamamoto, H., 2003. Isolation and developmental expression of tyrosinase family genes in *Xenopus laevis*. Pigment Cell Res. 16, 455–462.
Lacosta, A.M., Muniesa, P., Ruberte, J., Sarasa, M., Dominguez, L., 2005. Novel expression patterns of Pax3/Pax7 in early trunk neural crest and its melanocyte and non-melanocyte lineages in amniote embryos. Pigment Cell Res. 18, 243–251.
Lamb, T.M., Knecht, A.K., Smith, W.C., Stachel, S.E., Economides, A.N., Stahl, N., Yancopolous, G.D., Harland, R.M., 1993. Neural induction by the secreted polypeptide noggin. Science 262, 713–718.
Lang, D., Brown, C.B., Milewski, R., Jiang, Y.Q., Lu, M.M., Epstein, J.A., 2003. Distinct enhancers regulate neural expression of Pax7. Genomics 82, 553–560.
Le Douarin, N.M., Kalcheim, C., 1999. The neural crest. Cambridge university Press.
Le Grand, F., Rudnicki, M.A., 2007. Skeletal muscle satellite cells and adult myogenesis. Curr. Opin. Cell Biol. 19, 628–633.
Liem Jr., K.F., Tremml, G., Jessell, T.M., 1997. A role for the roof plate and its resident TGFbeta-related proteins in neuronal patterning in the dorsal spinal cord. Cell 91, 127–138.
Mansouri, A., Stoykova, A., Torres, M., Gruss, P., 1996. Dysgenesis of cephalic neural crest derivatives in Pax7−/− mutant mice. Development 122, 831–838.
Martin, B.L., Harland, R.M., 2001. Hypaxial muscle migration during primary myogenesis in *Xenopus laevis*. Dev. Biol. 239, 270–280.
Matsunaga, E., Araki, I., Nakamura, H., 2001. Role of Pax3/7 in the tectum regionalization. Development 128, 4069–4077.
McCauley, D.W., Bronner-Fraser, M., 2002. Conservation of Pax gene expression in ectodermal placodes of the lamprey. Gene 287, 129–139.
McGrew, L.L., Hoppler, S., Moon, R.T., 1997. Wnt and FGF pathways cooperatively pattern anteroposterior neural ectoderm in *Xenopus*. Mech. Dev. 69, 105–114.
McMahon, J.A., Takada, S., Zimmerman, L.B., Fan, C.M., Harland, R.M., McMahon, A.P., 1998. Noggin-mediated antagonism of BMP signaling is required for growth and patterning of the neural tube and somite. Genes Dev. 12, 1438–1452.
Meulemans, D., Bronner-Fraser, M., 2004. Gene-regulatory interactions in neural crest evolution and development. Dev. Cell 7, 291–299.
Minchin, J.E., Hughes, S.M., 2008. Sequential actions of Pax3 and Pax7 drive xanthophore development in zebrafish neural crest. Dev. Biol. 317, 508–522.
Mizuseki, K., Kishi, M., Matsui, M., Nakanishi, S., Sasai, Y., 1998. *Xenopus* Zic-related-1 and Sox-2, two factors induced by chordin, have distinct activities in the initiation of neural induction. Development 125, 579–587.
Monsoro-Burq, A.H., 2007. A Rapid Protocol for Whole-Mount In Situ Hybridization on *Xenopus* Embryos. Cold Spring Harbor. Protocols %R 10.1101/pdb.prot4809. 2007, pdb.prot4809-.
Monsoro-Burq, A.H., Bontoux, M., Vincent, C., Le Douarin, N.M., 1995. The developmental relationships of the neural tube and the notochord: short and long term effects of the notochord on the dorsal spinal cord. Mech. Dev. 53, 157–170.
Monsoro-Burq, A.H., Duprez, D., Watanabe, Y., Bontoux, M., Vincent, C., Brickell, P., Le Douarin, N., 1996. The role of bone morphogenetic proteins in vertebral development. Development 122, 3607–3616.
Monsoro-Burq, A.H., Fletcher, R.B., Harland, R.M., 2003. Neural crest induction by paraxial mesoderm in *Xenopus* embryos requires FGF signals. Development 130, 3111–3124.
Monsoro-Burq, A.H., Wang, E., Harland, R., 2005. Msx1 and Pax3 cooperate to mediate FGF8 and WNT signals during *Xenopus* neural crest induction. Dev. Cell 8, 167–178.
Nieuwkoop, P.D., Faber, J., 1994. Normal Table of *Xenopus laevis* (Daudin). Garland, New York.
Ny, A., Koch, M., Schneider, M., Neven, E., Tong, R.T., Maity, S., Fischer, C., Plaisance, S., Lambrechts, D., Heligon, C., Terclavers, S., Ciesiolka, M., Kalin, R., Man, W.Y., Senn, I., Wyns, S., Lupu, F., Brandli, A., Vleminckx, K., Collen, D., Dewerchin, M., Conway, E.M., Moons, L., Jain, R.K., Carmeliet, P., 2005. A genetic *Xenopus laevis* tadpole model to study lymphangiogenesis. Nat. Med. 11, 998–1004.
O'Neill, P., McCole, R.B., Baker, C.V., 2007. A molecular analysis of neurogenic placode and cranial sensory ganglion development in the shark, *Scyliorhinus canicula*. Dev. Biol. 304, 156–181.

Osorio, J., Mazan, S., Retaux, S., 2005. Organisation of the lamprey (*Lampetra fluviatilis*) embryonic brain: insights from LIM-homeodomain, Pax and hedgehog genes. Dev. Biol. 288, 100–112.

Read, A.P., Newton, V.E., 1997. Waardenburg syndrome. J. Med. Genet. 34, 656–665.

Relaix, F., Rocancourt, D., Mansouri, A., Buckingham, M., 2004. Divergent functions of murine Pax3 and Pax7 in limb muscle development. Genes Dev. 18, 1088–1105.

Relaix, F., Rocancourt, D., Mansouri, A., Buckingham, M., 2005. A Pax3/Pax7-dependent population of skeletal muscle progenitor cells. Nature 435, 948–953.

Rhinn, M., Dierich, A., Le Meur, M., Ang, S., 1999. Cell autonomous and non-cell autonomous functions of Otx2 in patterning the rostral brain. Development 126, 4295–4304.

Ridgeway, A.G., Skerjanc, I.S., 2001. Pax3 is essential for skeletal myogenesis and the expression of Six1 and Eya2. J. Biol. Chem. 276, 19033–19039.

Roche, D.D., Liu, K.J., Harland, R.M., Monsoro-Burq, A.H., 2009. Dazap2 is required for FGF-mediated posterior neural patterning, independent of Wnt and Cdx function. Dev. Biol. 333, 26–36.

Rupp, R.A., Weintraub, H., 1991. Ubiquitous MyoD transcription at the midblastula transition precedes induction-dependent MyoD expression in presumptive mesoderm of *X. laevis*. Cell 65, 927–937.

Sato, T., Sasai, N., Sasai, Y., 2005. Neural crest determination by co-activation of Pax3 and Zic1 genes in *Xenopus* ectoderm. Development 132, 2355–2363.

Sefton, M., Sanchez, S., Nieto, M.A., 1998. Conserved and divergent roles for members of the Snail family of transcription factors in the chick and mouse embryo. Development 125, 3111–3121.

Shapira, E., Marom, K., Yelin, R., Levy, A., Fainsod, A., 1999. A role for the homeobox gene Xvex-1 as part of the BMP-4 ventral signaling pathway. Mech. Dev. 86, 99–111.

Sharpe, C.R., Fritz, A., De Robertis, E.M., Gurdon, J.B., 1987. A homeobox-containing marker of posterior neural differentiation shows the importance of predetermination in neural induction. Cell 50, 749–758.

Sibthorpe, D., Sturlaugsdottir, R., Kristjansson, B.K., Thorarensen, H., Skulason, S., Johnston, I.A., 2006. Characterisation and expression of the paired box protein 7 (Pax7) gene in polymorphic Arctic charr (*Salvelinus alpinus*). Comp. Biochem. Physiol. B Biochem. Mol. Biol. 145, 371–383.

Sive, H.L., Grainger, R.M., Harland, R.M., 2000. Early Development of *Xenopus laevis*: a Laboratory Manual. Cold Spring Harbor Press, Cold Spring Harbor, N.Y.

Stutz, F., Spohr, G., 1986. Isolation and characterization of sarcomeric actin genes expressed in *Xenopus laevis* embryos. J. Mol. Biol. 187, 349–361.

Tamura, K., Dudley, J., Nei, M., Kumar, S., 2007. MEGA4: Molecular Evolutionary Genetics Analysis (MEGA) software version 4.0. Mol. Biol. Evol. 24, 1596–1599.

Tassabehji, M., Read, A.P., Newton, V.E., Harris, R., Balling, R., Gruss, P., Strachan, T., 1992. Waardenburg's syndrome patients have mutations in the human homologue of the Pax-3 paired box gene. Nature 355, 635–636.

Thompson, J.A., Zembrzycki, A., Mansouri, A., Ziman, M., 2008. Pax7 is requisite for maintenance of a subpopulation of superior collicular neurons and shows a diverging expression pattern to Pax3 during superior collicular development. BMC Dev. Biol. 8, 62.

Tour, E., Pillemer, G., Gruenbaum, Y., Fainsod, A., 2002a. Gbx2 interacts with Otx2 and patterns the anterior–posterior axis during gastrulation in *Xenopus*. Mech. Dev. 112, 141–151.

Tour, E., Pillemer, G., Gruenbaum, Y., Fainsod, A., 2002b. Otx2 can activate the isthmic organizer genetic network in the *Xenopus* embryo. Mech. Dev. 110, 3–13.

Tremblay, P., Pituello, F., Gruss, P., 1996. Inhibition of floor plate differentiation by Pax3: evidence from ectopic expression in transgenic mice. Development 122, 2555–2567.

Ye, W., Bouchard, M., Stone, D., Liu, X., Vella, F., Lee, J., Nakamura, H., Ang, S.L., Busslinger, M., Rosenthal, A., 2001. Distinct regulators control the expression of the mid–hindbrain organizer signal FGF8. Nat. Neurosci. 4, 1175–1181.